Journal of Environmental Management 356 (2024) 120753

Contents lists available at ScienceDirect

Journal of Environmental Management

journal homepage: www.elsevier.com/locate/jenvman

Promoting the circular economy: Valorization of a residue from industrial char to activated carbon with potential environmental applications as adsorbents

Ledicia Pereira [a], Ventura Castillo [a], Mónica Calero [a], Sergio González-Egido [b], M. Ángeles Martín-Lara [a,**], Rafael R. Solís [a,*]

[a] Department of Chemical Engineering, University of Granada, Avda. Fuentenueva s/n, 18071, Granada, Spain
[b] Environment and Bioproducts Group, Department of Life Sciences, University of Alcalá, Alcalá de Henares, 28871, Madrid, Spain

ARTICLE INFO

Handling editor: Jason Michael Evans

Keywords:
Char
Activated carbon
Adsorption
Carbon dioxide
Heavy metals
Pharmaceuticals

ABSTRACT

Pyrolysis of residues enriched with carbon, such as in agroforestry or industrial activities, has been postulated as an emerging technology to promote the production of biofuels, contributing to the circular economy and minimizing waste. However, during the pyrolysis processes a solid fraction residue is generated. This work aims to study the viability of these chars to develop porous carbonaceous materials that can be used for environmental applications. Diverse chars discharged by an industrial pyrolysis factory have been activated with KOH. Concretely, the char residues came from the pyrolysis of olive stone, pine, and acacia splinters, spent residues fuel, and cellulose artificial casings. The changes in the textural, structural, and composition characteristics after the activation process were studied by N_2 adsorption-desorption isotherms, scanning electron microscopy, FTIR, elemental analysis, and XPS. A great porosity was developed, S_{BET} within 776–1186 $m^2\ g^{-1}$ and pore volume of 0.37–0.59 $cm^3\ g^{-1}$ with 70–90% of micropores contribution. The activated chars were used for the adsorption of CO_2, leading to CO_2 maximum uptakes of 90–130 mg g^{-1}. There was a good correlation between the CO_2 uptake with microporosity and oxygenated surface groups of the activated chars. Moreover, their ability to adsorption of contaminants in aqueous solution was also evaluated. Concretely, there was studied the adsorption of aqueous heavy metals, i.e., Cd, Cu, Ni, Pb, and Zn, and organic pollutants of emerging concern such as caffeine, diclofenac, and acetaminophen.

1. Introduction

The growing recognition of the environmental challenges faced by our planet has led to a heightened focus on understanding and mitigating two critical issues: the excessive release of carbon dioxide into the atmosphere (Odunlami et al., 2022) and water scarcity (Ungureanu et al., 2020). The presence of pollutants in water bodies such as heavy metals (Mukherjee et al., 2021) or anthropogenic organic contaminants of emerging concern (Kasonga et al., 2021) like pharmaceuticals and or personal care products hazards the reuse of wastewater effluents (Kümmerer et al., 2018). These issues have significant implications for the health of ecosystems, human well-being, and the sustainability of our natural resources (Fuller et al., 2022). All these pollutants pose a significant threat to water and air quality, putting the well-being of both wildlife and human populations on the line. It is imperative to mitigate their release and decontaminate them to uphold a state of optimal health among the population and lessen the global mortality rates attributed to air and water pollution. In 2019 alone, air pollution was responsible for approximately 6–7 million premature deaths worldwide, while water pollution contributed to 1–4 million premature deaths (Fuller et al., 2022).

The worldwide energy-related CO_2 emissions were reported to have stayed constant at 36.1 Gt (Liu et al., 2023) but had a significant impact on the global annual average of atmospheric CO_2 concentration, leading to a rise of approximately 2.6 parts per million in 2020 (Hong, 2022). Strategies for reducing atmospheric CO_2 concentrations include the use of renewable energy sources (Saleem et al., 2022), energy optimization (Nakkasunchi et al., 2021), growing natural forests (Manning, 2010),

* Corresponding author.
** Corresponding author.
E-mail addresses: marianml@ugr.es (M.Á. Martín-Lara), rafarsolis@ugr.es (R.R. Solís).

https://doi.org/10.1016/j.jenvman.2024.120753
Received 20 October 2023; Received in revised form 6 March 2024; Accepted 20 March 2024

and sequestration by diverse processes, in which absorption using amine-based solvents is currently the most used technique (Akeeb et al., 2022). However, the adsorption technique is emerging as an economical and greener alternative for capturing and storing the emitted CO_2 from industrial activity (Akeeb et al., 2022; Quan et al., 2023).

On the other hand, anthropogenic and intensified industrialization activities exert a direct influence on the contamination of water bodies by heavy metals and organic pollutants. Heavy metal contamination predominantly originated from direct effluent emissions into rivers and lakes coming from industrial discharges, power generation, mining operations, battery manufacturing facilities, paper mills, petrochemical industries, paint manufacturing units, and similar sources (Wang et al., 2022a; Rathi et al., 2021). These heavy metals encompass cadmium, copper, zinc, lead, nickel, and chromium (Rathi et al., 2021). Various techniques exist for the elimination of harmful metallic ions, such as ion exchange, inverse filtration, precipitate separation, adsorption, coagulation, and extraction (Baby et al., 2019; López et al., 2023; Liu et al., 2018; Muya et al., 2016). In addition, organic dyes, pharmaceuticals, and personal care products, along with others related to modern life are also prevalent in wastewater as a result of human activities (Yadav et al., 2021). For instance, caffeine has been found in Italian and German natural waters at maximum concentrations, respectively, of 124 ng L^{-1} (Loos et al., 2007) and 640 μg L^{-1} (Heberer, 2002). Diclofenac, a widely spread anti-inflammatory pharmaceutical, is consumed at a rate of approximately 1000 tons annually and has been detected in surface, ground, and drinking water at concentrations ranging from ng/L to μg/L (Lonappan et al., 2016). Diclofenac is considered a prevalent environmental contaminant in various regions worldwide, including Switzerland, Spain, Sweden, and the Baltic region (Lonappan et al., 2016). Acetaminophen is a pharmaceutical compound used as a painkiller, for fever reduction, and analgesic purposes. The global consumption of acetaminophen exceeded 149.3 kilotons in 2014, and it has frequently been detected in water sources (Pylypchuk et al., 2018; Phong Vo et al., 2019).

Adsorption processes have emerged as a greener alternative that avoids the use of toxic solvents for capturing CO_2 from gas effluents (Quan et al., 2023; Pérez-Huertas et al., 2023) and the removal of water contaminants (Srivastava et al., 2021; Li et al., 2020). These processes have garnered attention for their remarkable effectiveness, respect for the environment, ease of implementation, affordability, and exceptional efficiency (jia Liu et al., 2018; Lu et al., 2017). The most utilized adsorbents include carbon materials, and zeolites, as well as recently metal-organic frameworks (MOFs) and ionic liquids, among others. MOFs are highly porous materials constructed from metal ions or clusters coordinated with organic ligands (Huang et al., 2021). Although MOFs exhibit exceptional adsorption capacities, their synthesis often involves complex and costly procedures. Moisture can hinder the accessibility of adsorption sites within zeolitic structures, limiting their effectiveness (Resasco et al., 2021). Ionic liquids, characterized by their liquid state at room temperature, possess unique properties that make them attractive for the absorption of gases such as CO_2 (Ramos et al., 2020). Their high cost and difficulty in managing and utilizing ionic liquids can hinder their widespread implementation (Huang and Rther, 2009). Therefore, carbon materials emerge as the most favorable alternative for the removal of both CO_2 and water pollutants due to their well-established properties, low cost, effectiveness, and versatility in adsorption processes (Guo et al., 2022; Ghanbarpour Mamaghani et al., 2023). Notably, residual biomass and non-recyclable plastics hold remarkable potential as sources of carbon for producing biochar through pyrolysis processes (Pérez-Huertas et al., 2023). These materials are abundantly available in nature, stemming from agricultural, forestry, and human-related activities, making them valuable renewable sources of carbon with environmentally friendly characteristics (jia Liu et al., 2018; Lu et al., 2017; Huang et al., 2021). Diverse residues rich in carbon content have been successfully transformed into carbonaceous adsorbents. Just to cite some examples, winery wastes (Sellaoui et al., 2021), residues from the mushroom production chains (Lazarotto et al., 2021), sludge from urban wastewater treatment (Pigatto et al., 2020), sludge from the brewery industry (Streit et al., 2021), or agroforestry residues (Salomón et al., 2021; Kerkhoff et al., 2021; Georgin et al., 2021).

This work deals with the assessment of the adsorption effectiveness of porous activated carbon materials prepared from the chemical activation of industrial char that utilize newly developed processed plastics and forestry residues as effective strategies for the removal of CO_2 and water decontamination. Diverse industrial chars discharged after the pyrolysis process to obtain biofuels were considered. In particular, the chars came from the pyrolysis of forestry residues such as olive stone, pine, and acacia splinters, solid recovered fuel (SRF), and cellulose artificial casings. Olive stones proceeded from the olive oil industry; pine and acacia splinters were residues from agroforestry activities; the SRF comes from the dehydration of solid waste, typically consisting of combustible components of municipal solid waste; and cellulose artificial casings are artificial viscose casings widely used in the food industry. These residues were pyrolyzed in a local factory to prevent them from being landfilled, which led to obtaining added-value biofuels. In the process, also a char was obtained, which was the object of this investigation. Hence, the valorization of this pyrolysis residue into an activated carbonaceous material enables to closing of the recycling loop.

Diverse chemical agents have been lately researched to activate carbon precursors, paying special attention to low hazardous substances (Sevilla et al., 2021). Nonetheless, KOH is the most popular studied to date due to its superior reactivity towards carbon (Gao et al., 2020), leading, therefore, to utmost performance in developing microporosity (Dziejarski et al., 2023). The activated chars were fully characterized and their properties were analyzed by N_2 physisorption, FTIR, and elemental analysis. The activated chars were then examined for the adsorption of CO_2 from gaseous streams, removal of aqueous heavy metals (Cd, Cu, Ni, Pb, and Zn), and organic pollutants of emerging concern (caffeine, diclofenac, and acetaminophen).

2. EXPERIMENTAL section

2.1. Activation of the industrial chars

The industrial chars were obtained from local factories that produce syngas and biofuels from the pyrolysis of municipal, industrial, and agroforestry residues. Five different chars of different nature were provided, i.e. olive stone (OS), industrial first-transformation agroforestry waste products like pine or acacia splinter, and industrial wastes such as the solid recovered fuel (SRF) or cellulose artificial casings. The five collected chars were dried overnight at 120 °C. The activation was carried out with KOH due to the highest textural properties developed (Ligero et al., 2023). The thermal activation started by placing in an inert crucible the char and KOH at a mass ratio of 1:1 based on the conditions studied in a previous work (Ligero et al., 2023). The thermal treatment was carried out under inert N_2 fed at 200 mL min^{-1}. The char-KOH mixture was heated from room temperature to 300 °C at a rate of 10 °C min^{-1}. After, the temperature was held for 1 h at 300 °C to melt the activating agent. Next, the temperature rose from 300 °C to 800 °C at a rate of 10 °C min^{-1}. Then, the temperature was kept for 1 h at this temperature. Finally, the sample was cooled to room temperature. The cooled samples were then washed with 1 M HCl and dried at 120 °C overnight. The dried solid was ground and sieved to <250 μm. The final activated chars were named OS-AC (from olive stone), Pine-AC (from pine splinters), Acacia-AC (from acacia splinters), SRF-AC (from spent residue fuels) and Cellulose-AC (from cellulose artificial casings). The yield of the activated carbon during their preparation was 79% for OS-AC, 75% for Pine-AC, 72% for Acacia-AC, 41% for SRF-AC, and 78% for Cellulose-AC. A commercial powder-activated carbon purchased from Panreac AppliChem has been used for comparison purposes.

2.2. Characterization of the chars

The textural properties were studied by N_2 physisorption. The adsorption-desorption isotherms with N_2 at 196 °C were obtained in a Sync 200 device from 3P Instruments©. The samples were degassed overnight at 150 °C under a vacuum in a J4 prep degasser station of 3P Instruments©. The specific surface area was obtained by the Brunauer-Emmett-Teller method (S_{BET}, relative standard deviation RSD <1%), and the total specific pore volume (V_T) was calculated from the N_2 uptake at p/p_0~0.99. The t-plot method was used for the estimation of the specific surface of micropores (S_{MP}) and the micropore volume (V_{MP}). The micropore size distribution was obtained by CO_2 adsorption isotherms carried out at 0 °C, considering the Horvath–Kawazoe (HK) method for the calculation (Gauden et al., 2004; Dombrowski et al., 2001).

The proximate analysis was applied to quantify the percentages of moisture, volatiles, fixed carbon, and ash in the samples by thermogravimetric analysis in a PerkinElmer STA 6000 thermobalance (RSD <5%). The sample was first kept at 30 °C under N_2 (20 mL min^{-1}). Next, the temperature was risen to 110 °C (heating rate, 40 °C min^{-1}) and maintained for 10 min at this temperature. Then, the temperature was raised to 875 °C (heating rate, 40 °C min^{-1}) and kept at this temperature for 10 min. Finally, the N_2 was changed into O_2 (20 mL min^{-1}) at 875 °C for another 10 min. The determination of each of the constituents was completed by quantifying the weight loss in each step, and the fixed carbon by the difference.

The morphology of the particles was observed by Scanning Electron Microscopy (SEM) in a FEI Quanta 400 device (30 kV, 3.5 nm resolution).

The content of carbon, hydrogen, nitrogen, and sulfur was determined by elemental analysis in a Thermo Scientific Flash 2000 device (RSD values, 0.5% for C, 1% for H, and 0.6% for N). Oxygen was estimated by the difference with the other elements after the removal of the ash content from the proximate analysis. For the chemical composition of the surface, X-ray Photoelectron Spectroscopy (XPS) was carried out in a Kratos AXIS Ultra-DLD device using an X-ray source from Al Kα. All the spectra were corrected to the C1s peak of adventitious carbon to 284.6 eV. For the processing and deconvolution of the peaks, the software XPSpeak 4.1® was used, considering a Shirley background correction.

2.3. Adsorption tests

2.3.1. Adsorption of CO_2

The adsorption of CO_2 was assessed in terms of thermodynamics and kinetics. The thermodynamics of CO_2 adsorption was carried out through physisorption in a Sync 200 device from 3P Instruments©. As done with N_2 isotherms, the samples underwent the same pretreatment procedure. The adsorption isotherms were conducted at 0 °C and 25 °C, and the data obtained fitted to a Freundlich isotherm, in which the CO_2 uptake (q_{CO2}, mg g^{-1}) is described as a function of the CO_2 pressure (p) as follows (Freundlich, 1907):

$$q_{CO_2} = K_F\, p^{1/n_F} \quad (1)$$

where K_F (mg g^{-1} kPa^{-nF}) and n_F are, respectively, the Freundlich constant and exponent. The CO_2/N_2 selectivity during the CO_2 process was calculated from their respective isotherms conducted at 25 °C, applying the Henry's law, by dividing the initial slopes of CO_2 and N_2 adsorption isotherms (Wang et al., 2022b). The isosteric heat of CO_2 adsorption (ΔH_{ads}) was obtained as a function of the CO_2 uptake (q_{CO2}) applying the Clausius–Clapeyron equation (Nuhnen and Janiak, 2020; He et al., 2021):

$$\Delta H_{ads} = -R \ln\left(\frac{P_2}{P_1}\right)\frac{T_1 T_2}{(T_2 - T_1)} \quad (2)$$

Fixing a value for the CO_2 uptake, the pressure (p_1 and p_2) was obtained using the parameters obtained with the Freundlich model at T_1 = 0 °C and T_2 = 25 °C, leading to the obtention of the isosteric adsorption calculation.

The kinetics of adsorption of CO_2 was assessed in thermobalance (PerkinElmer, STA 6000) assays following a three-step program. The first step consisted of a drying step by heating the sample from room temperature to 200 °C, and kept for 1 h, under 50 mL min^{-1} of N_2. The second step was a cooling of the sample from 200 °C to 30 °C under 50 mL min^{-1} of N_2. Finally, the isothermal CO_2 adsorption of the dried sample was conducted under 50 mL min^{-1} of CO_2 for 2 h, until a constant sample mass was reached. During the adsorption of CO_2, the mass of the sample increased from the initial mass of the dried sample. This increase lets the determination of the adsorbed CO_2 capacity over time (q_{CO2}). The CO_2 adsorption kinetics have been adjusted to two models that are usually applied to physisorption processes (Wang and Guo, 2020; Ammendola et al., 2017). Lagergren's pseudo-first order model supposes that the rate of CO_2 adsorption is directly proportional to the difference between the saturation concentration and the mean concentration within the particle, describing the evolution of the adsorbed CO_2 capacity (q_{CO2}, mg g^{-1}) as follows (Díez et al., 2015):

$$q_{CO_2} = q_1\left(1 - e^{-k_1 t}\right) \quad (3)$$

where q_1 (mg g^{-1}) means the CO_2 adsorption capacity at saturation conditions of the pseudo-first order model and k_1 (min^{-1}) is the pseudo-first order rate constant. The Avrami model is a three-parameter modification of the first-order kinetics that was originally proposed to model the phase transitions and crystal growth of materials (Avrami, 1939) but has been recently applied to the study of CO_2 adsorption onto functionalized activated carbon (Shafeeyan et al., 2015; Serna-Guerrero and Sayari, 2010; Kaur et al., 2019). The Avrami model predicts the adsorption evolution by a fractal modification of the pseudo-first order of the adsorbed CO_2 as follows:

$$q_{CO_2} = q_A\left(1 - e^{-(k_A t)^{n_A}}\right) \quad (4)$$

where q_A (mg g^{-1}) means the CO_2 adsorption capacity at saturation conditions of the Avrami model, k_A (min^{-1}) is the Avrami kinetic constant and n_A (dimensionless) is the Avrami exponent.

2.3.2. Adsorption of aqueous heavy metals and contaminants of emerging concern

The batch adsorption experiments of heavy metals were conducted in 100 mL Erlenmeyer flasks at room temperature (25 °C). Different solutions of Pb, Zn, Ni, Cd, and Cu within approximately 10–300 mg L^{-1} with an adsorbent dose of 2.0 g L^{-1} and 160 rpm in an orbital stirrer until reaching the equilibria. The samples were filtered with syringe filters (Millipore Millex-GV PVDF, 0.45 μm), and the concentration of the metal was analyzed by Atomic Absorbance (AA) spectrometry in a PerkinElmer® PinAAcle 500 Flame device. The initial concentration of the metallic adsorbate solution before adding the adsorbent and after reaching the equilibria was analyzed for the determination of the adsorption uptake.

The batch adsorption experiments of the organic contaminant of emerging concern followed the same procedure conducted with the heavy metals. Different solutions of caffeine (CAF), diclofenac (DCF), and acetaminophen (ACE) within 10–500 mg L^{-1} with an adsorbent dose of 0.2–2.0 g L^{-1} and 200 rpm of magnetic stirring. The concentration of the organic was quantified by High-Pressure Liquid Chromatography (HPLC) in an Alliance e2695 HPLC device from Waters™ coupled to a 2998 photodiode array UV–visible detector. The stationary phase used for the separation was a Zorbax Bonus-RP column (4.6 × 150 mm, 5 μm). For the analysis of CAF and DCF, isocratic methods were carried out. A mixture of acetonitrile (A) and acidified water with 0.1% (vol.) of trifluoroacetic acid (B) was pumped at a rate of 1 mL min^{-1} with

an A:B ratio of 15:85 for CAF and 65:35 for DCF. In the case of ACE, a gradient method was applied from 20:80 to 60:40 in 7 min. The quantification was conducted at 275 nm for CAF, 247 nm for DCF, and ACE.

The isotherms of aqueous contaminants, either metals or organic pollutants of emerging concern, were fitted to different models (Mozaffari Majd et al., 2022). It was the three-parameter model such as the Sips equation, which better fitted to the experimental data than the two parameters Freundlich (1907) or Langmuir (1918) model. Sips's equation describes the isotherm as follows (Sips, 1948):

$$q_e = \frac{q_S (K_S C_e)^{n_S}}{1 + (K_S C_e)^{n_S}} \quad (5)$$

where q_e (mg g^{-1}) and q_S (mg g^{-1}) are the adsorbed amount in the equilibria and the maximum, respectively; K_S (mg^{-1} g) is the Sips's constant and n_S (dimensionless) the Sips's exponent.

The adsorption kinetics of the aqueous contaminants have been adjusted to two models that are usually applied to physisorption processes (Tan and Hameed, 2017). From all of them, the pseudo-second order was selected due to the best-fitting results achieved. The Ho's pseudo-second order assumes that the sorption uptake is proportional to the number of active sites occupied on the sorbent modeling the temporal adsorbed contaminant (q_t, mg g^{-1}) as follows (Ho and McKay, 1999):

$$q_t = \frac{k_2 q_2^2 t}{1 + k_2 q_2^2 t} \quad (6)$$

where q_2 (mg g^{-1}) means the contaminant adsorption capacity at saturation conditions obtained by the pseudo-second order and k_2 (mg^{-1} g min^{-1}) is the pseudo-second order rate constant.

3. Results and discussion

3.1. Characterization of the activated chars

The analysis of the textural properties was considered the key proof of the activation of the chars and the building of a porous material with empowered adsorption properties. The main results of N_2 isotherms at 77 K are provided in Table 1, and Fig. 1A depicts the adsorption-desorption isotherms of the activated materials. The raw materials, which means the chars before activation, were non-porous, BET areas reached values of 12 m^2 g^{-1} (Acacia-char) or 23 m^2 g^{-1} (SRF-char) or even below. The activation with KOH provided a great porosity, raising the surface area from 779 m^2 g^{-1} (Pine-char) to over 1000 m^2 g^{-1} (OS-AC and acacia-AC). These results are similar to the porosity reported in the literature by KOH for biochars (Sakhiya et al., 2020) and other residues based on plastics (Pérez-Huertas et al., 2023), which are very competitive to commercial formulas such as thatshown in Fig. 1A with roughly 713 m^2 g^{-1}. The N_2 isotherms can be identified, according to IUPAC's classification (Bläker et al., 2019), as Type I for all the samples except for SRF-AC, defining a concave inflection point at p/p_0~0.1. Type I is ascribed to microporous materials, having pore size distributions over a broad range since the inflection point is displaced from p/p_0 = 0.1 (Bläker et al., 2019; Sing et al., 1985). The sample SRF-AC described a mixed isotherm of Types I and IV, providing evidence of certain mesoporosity (Sing et al., 1985). The samples that defined a Type I isotherms did not describe any hysteresis loop since the desorption step overlaps the adsorption curve. However, the SRF-AC sample did perform a type H4 hysteresis, characteristic of micro-mesoporous carbon materials (Sing et al., 1985), also associated with narrow slit mesopores (Alothman, 2012). The microporosity was high in all the samples, much more important than the commercial formula (only 33% of micropores), as the proportion of micropore volume to the total was around 90%, except for SRF-AC which provided only 71% of micropores. Regarding the size of the micropore, the HK method was applied to the CO_2 adsorption isotherms carried out at 0 °C, leading to the size distribution depicted in Fig. 1B. As observed, the micropore size most frequently was around 0.5–0.7 nm which is consonant with the activation of KOH according to the literature (Wei et al., 2019).

The textural morphology of the particles after activation was visually confirmed by SEM micrographs. Fig. 2 illustrates a selection of the pictures taken for the five activated chars. The images provide evidence of the porosity developed in the material. Due to the vegetal origin of olive stones, pine, and acacia splinters, the structure of the activated chars still resembles their origin. In the case of olive stone, a porous structure resembling a sponge is envisaged. For pine and acacia, a brick shape is identified in which long organized, and repeated slits are defined. The action of KOH during activation promotes the formation of additional cavities, as observed in the case of pine (Fig. 2C) in which small holes are defined in the lateral wall of the particle, probably during the activation reaction of the organic content of the char and KOH. In the case of Cellulose-AC and SRF-AC, some cavities were also observed. In the case of the plastic cellulose casing, the activated material displayed cavities and holes as the result of a combination of plain surfaces. The SRF-AC was the material with the highest heterogeneity observed. Although a holey morphology is frequently observed, there were also appreciated wrinkled and granulated surfaces.

The results of proximate and elemental analysis are provided in Table 2. The chars were characterized by a high carbon content in the case of Pine-char, Acacia-char, and Cellulose-char, as they are the result of a pyrolysis process of biomass precursors, leading to over 80% of carbon content. Pine residues have been reported to lead the formation of char with over 89% of C (Kim et al., 2012; Huff et al., 2014); acacia wood usually leads to chars with C percentage up to 70% (Ahmed et al., 2018), and in the case of cellulose the C content can reach values close to 90% (Fan et al., 2021). OS-char is frequently reported by a lower carbon content (Gil et al., 2015) as a consequence of the C percentage of the olive stones, frequently around 50% (García Martín et al., 2020). SRF-char also displayed lower C content, due to its complex origin, with an important contribution of inorganic matter as the high ash content suggests. The content of nitrogen, if detected, was low in all the chars except the almost 2% found in the SRF-char. The oxygen was obtained as the difference in the elemental analysis; leading to considerable percentages in OS-char and SRF-char. However, the high content of ash obtained in these samples suggests an important content of inorganic matter. In general terms, there is a good relationship between the fixed carbon of proximate analysis and the carbon content obtained by elemental analysis, being the pine-char, acacia-char, and cellulose-char the most carbon enriched. The activation with KOH enriched the carbon content and reduced the ash proportion. KOH has been reported as capable of dissolving ash and other compounds during the activation (Li et al., 2022), that were removed during the washing carried out after the activation (Kozyatnyk et al., 2021).

Table 1
Textural properties obtained from N_2 adsorption-desorption isotherms.

Sample	S_{BET} (m^2 g^{-1})	S_{MP} (m^2 g^{-1})	V_T (cm^3 g^{-1})	V_{MP} (cm^3 g^{-1})	V_{MP}/V_T (%)
OS-char	<0.1	0	<0.001	0	0
Pine-char	0.4	0	0.002	0	0
Acacia-char	12.3	0	0.024	0	0
SRF-char	22.7	1.4	0.062	0	0
Cellulose-char	1.4	0	0.005	0	0
OS-AC	1186.8	1131.5	0.646	0.595	92.1
Pine-AC	778.7	718.6	0.424	0.373	87.9
Acacia-AC	1030.1	973.1	0.562	0.511	90.9
SRF-AC	824.6	732.6	0.539	0.384	71.2
Cellulose-AC	966.0	919.8	0.531	0.484	91.1
Commercial AC	712.8	396.3	0.625	0.204	32.6

S_{BET}: total specific surface area by BET method; S_{MP}: micropore surface area by t-plot method; V_T: total pore volume from N_2 uptake at p/p_0~0.99; V_{MP}: micropore volume by t-plot method.

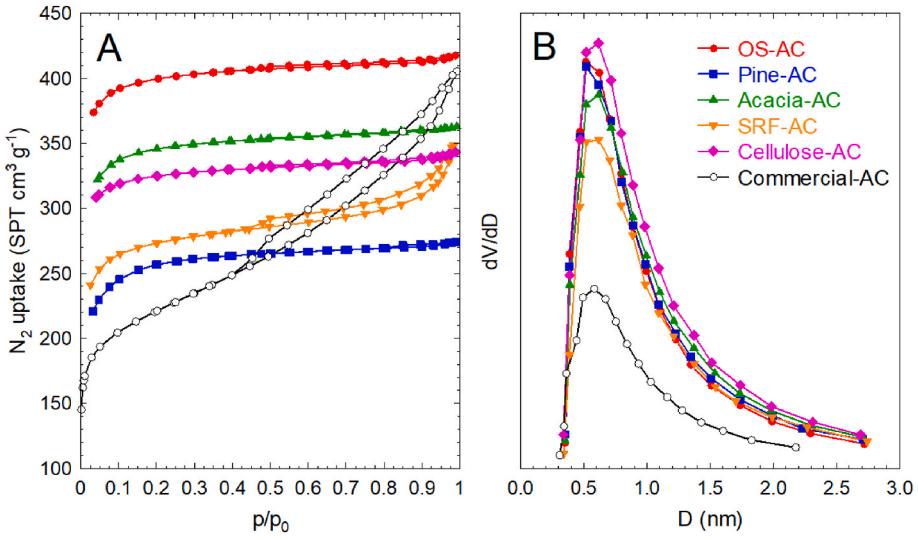

Fig. 1. N_2 adsorption-desorption isotherms of the industrial chars after activation (A) and micropore size distribution obtained by the HK method from CO_2 adsorption isotherms (B).

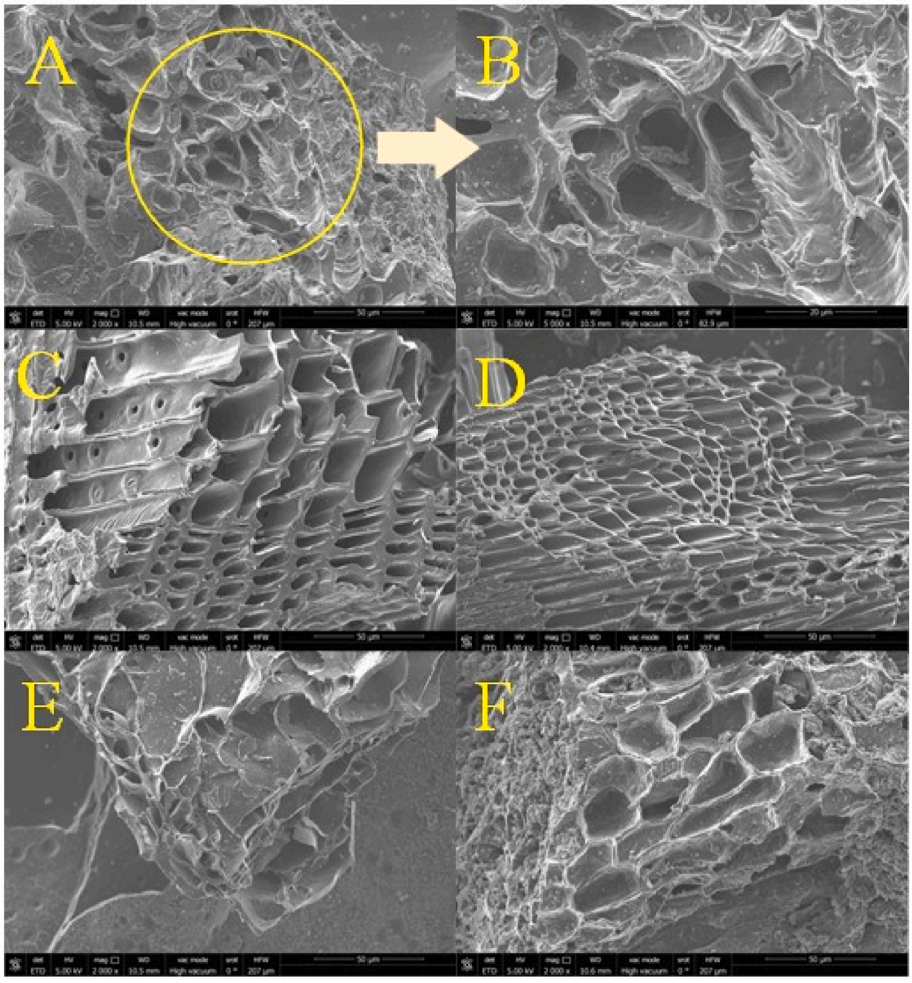

Fig. 2. SEM pictures of the chars after activation: OS-AC (A and B), Pine-AC (C), Acacia-AC (D), Cellulose-AC (E), and SRF-AC (F).

The chemical composition of the surface was assessed by the XPS technique. Table 3 summarizes the results of elemental composition and the characterization of the chemical environment of C, and O, i.e. the nature of the functional groups on the surface. Some differences are stated when comparing the results obtained by XPS and elemental analysis. For instance, the contribution of C is lower in the case of XPS. Bearing in mind the superficial character of the XPS technique, this effect provides evidence of the presence of oxygen groups, concentrated

Table 2
Proximate and elemental analysis of the chars before and after activation.

Sample	Proximate analysis (wt. %)				Elemental analysis (wt.%)			
	Moisture	Volatile	Fixed carbon	Ash	N	C	H	O[a]
OS-char	1.4	12.9	81.4	4.3	0.2	60.3	16.2	19.0
Pine-char	3.1	15.8	77.5	3.6	–	85.9	4.4	6.1
Acacia-char	3.5	14.9	80.1	1.5	0.4	83.5	3.8	10.7
SRF-char	2.7	14.6	52.2	30.5	1.9	61.7	3.4	2.6
Cellulose-char	1.9	14.6	81.4	2.1	–	84.9	3.9	9.1
OS-AC	4.7	8.3	85.0	2.0	–	89.0	0.2	8.9
Pine-AC	3.1	13.0	81.2	2.7	–	84.3	0.3	12.7
Acacia-AC	5.4	11.0	81.9	1.7	0.6	86.4	0.3	11.0
SRF-AC	7.6	9.1	69.5	13.8	0.9	74.8	0.4	10.2
Cellulose-AC	8.9	12.6	78.5	0	0.2	88.6	0.2	11.0
Commercial-AC	0.7	5.3	93.2	0.8	0.5	89.0	0.3	9.9

[a] Obtained as the difference after removing the ash content.

Table 3
Surface chemical composition of the activated chars by XPS.

Sample	C_{XPS}	O_{XPS}	N_{XPS}	$Others_{XPS}$	C_{1s}				O_{1s}		
	(wt.%)				Type	BE (eV)	% Peak	C_{XPS}-Ox (wt.%)	Type	BE (eV)	% Peak
OS-AC	73.9	15.9	3.5	4.0 (Fe)	C═C	284.6	47.0	17.1	quinone	530.7	0.0
				1.2 (Si)	C–C	285.2	30.5		C═O	531.7	58.3
				1.1 (Ca)	C–O	286.5	0.6		C–O	533.4	41.7
				0.3 (Zn)	C═O	287.9	14.1				
					COO-	290.0	8.5				
Pine-AC	71.3	22.4	0.4	2.8 (K)	C═C	284.6	49.2	15.6	quinone	531.0	9.7
				2.6 (Ca)	C–C	285.4	29.2		C═O	531.7	52.3
				0.2 (Si)	C–O	286.6	0.0		C–O	533.5	38.1
					C═O	288.5	21.9				
					COO-	289.9	0.0				
Acacia-AC	67.3	23.2	0.9	3.1 (Fe)	C═C	284.5	58.5	18.0	quinone	531.0	22.1
				2.4 (Ca)	C–C	285.2	14.7		C═O	531.8	38.1
				2.4 (K)	C–O	286.5	8.8		C–O	533.3	39.7
					C═O	288.5	10.0				
					COO-	289.9	8.0				
SRF-AC	48.9	28.1	1.4	7.9 (Si)	C═C	284.5	60.3	15.1	quinone	530.8	12.7
				4.5 (Fe)	C–C	285.7	8.7		C═O	532.1	44.3
				3.5 (Ti)	C–O	286.5	10.8		C–O	533.0	43.9
				2.7 (K)	C═O	288.5	15.8				
				1.5 (P)	COO-	289.9	4.3				
Cellulose-AC	80.6	14.0	0.6	4.4 (Fe)	C═C	284.5	64.2	21.2	quinone	530.8	23.4
				0.5 (Ca)	C–C	285.4	9.5		C═O	532.0	37.9
					C–O	286.2	9.3		C–O	533.4	38.7
					C═O	288.1	6.6				
					COO-	289.5	10.4				
Commercial-AC	94.5	5.5	–	–	C═C	284.6	64.0	24.6	quinone	530.7	10.6
					C–C	285.7	9.9		C═O	532.1	26.3
					C–O	286.4	6.4		C–O	533.5	63.1
					C═O	288.5	5.5				
					COO-	290.0	14.1				

onto the surface. The O percentages provided by XPS were higher than those tentatively estimated by elemental analysis. The chemical nature of the elements at the surface was assessed by deconvolution of the high-resolution XPS spectra. Regarding the C_{1s} spectra, the following contributions were considered for deconvolution: C═C (284.6 eV), C–C (285.3 eV), C–O (286.6 eV), C═O (288.0 eV), and O═C-OR (289.9 eV) (Ramírez-Valencia et al., 2023). The O_{1s} region was fitted to quinone (530.7 eV), C═O (531.5–532.0 eV), and C–O (~533 eV) (Burg et al., 2002). The N, although detected, was not deconvoluted due to the low proportion at which it appeared. Table 3 also summarizes the elemental composition of the surface of the activated chars. In this table, it can be observed that the carbon content decreased in the order Cellulose-AC > OS-AC ~ Pine-AC > Acacia-AC > SRF-AC. The carbon content varies from the values obtained by elemental analysis; nevertheless, the XPS analysis accounts only superficially, not the whole bulk of the particle as in elemental analysis. The deconvolution analysis of the C_{1s} region is depicted in Fig. 3, in which it can be appreciated a similar distribution of functional groups with some exceptions such as the lack of C–O in OS-AC and Pine-AC or the high proportion of carboxylic groups in Cellulose-AC, Acacia-AC, and OS-AC. However, due to the different content of carbon in each sample, the comparison should be taken with caution. For an accurate evaluation of the percentage of oxygenated carbonaceous groups, the sum of percentages of the area of the peaks regarding oxygenated groups, i.e. C–O, C═O, and COO^{-}, from C_{1s} region was multiplied by the carbon content. According to this calculation (see C_{XPS}-Ox column in Table 3), the percentages of C_{XPS}-Ox decreased in the order Cellulose-AC > Acacia-AC > OS-AC > Pine-AC ~ SRF-AC. The O_{1s} region was also deconvoluted, considering that the oxygen is linked to carbon exclusively. However, as pointed out in Table 3, the amount of metal content cannot be considered negligible. These metals are expected to be oxides. For this reason, the results of O_{1s} deconvolution (see Fig. 3) are just a mere qualitative comparison between functional groups, out of any feasible quantification. Interestingly, in the case of OS-AC the presence of quinonic groups was not observed. Acacia-AC and Cellulose-AC displayed an equilibrated proportion of quinonic, C–O, and C═O groups. In the case of Pine-AC and SRF-AC, the proportion of

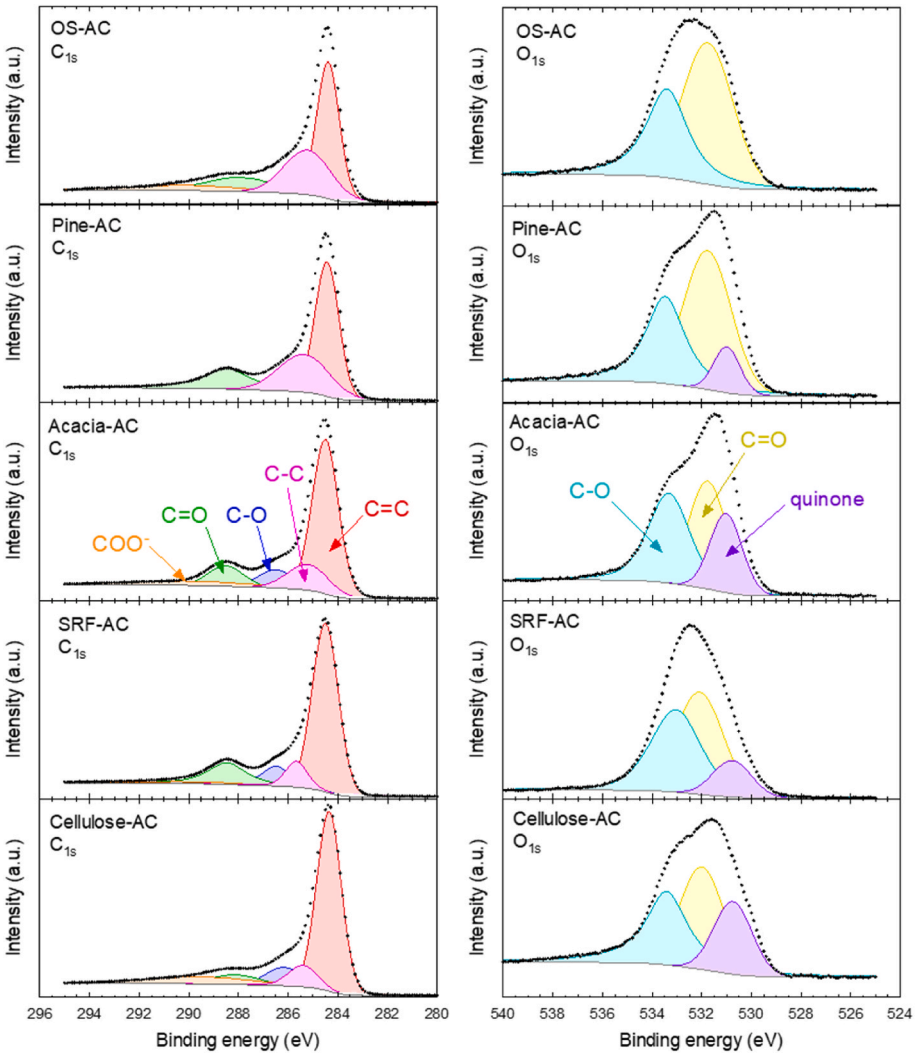

Fig. 3. XPS deconvolution of the C_{1s} (left) and O_{1s} (right) regions of the activated chars.

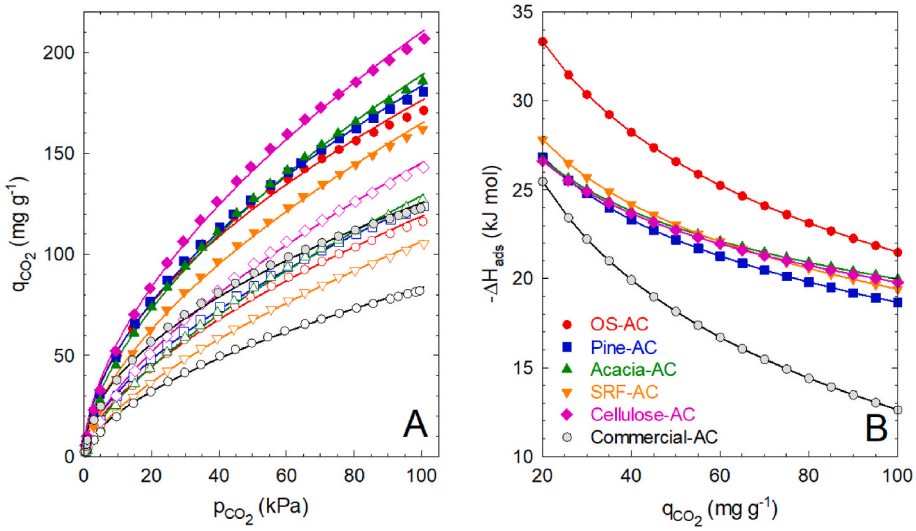

Fig. 4. (A) CO_2 adsorption isotherms at different pressures at 0 °C (filled symbols) and 25 °C (empty symbols). (B) Isosteric heat of adsorption (ΔH_{ads}).

functional groups was C═O > C–O > quinonic groups.

3.2. Adsorption of CO_2

The thermodynamics of CO_2 adsorption was first studied at different pressures up to 100 kPa at two different temperatures, i.e. 0 °C and 25 °C, see the results depicted in Fig. 4A. The continuous growth tendency of the CO_2 uptake until 100 kPa suggests a good fitting to the Freundlich isotherms that lack the definition of a plateau, confirmed by the good correlation coefficient ($R^2 > 0.99$, see results in Table 4). The Freundlich model is an empirical model that assumes a non-ideal and reversible process of plausible multilayer adsorption on a heterogeneous surface (Freundlich, 1907), due to the presence of certain heterogeneity in the surface of the material (Serafin and Dziejarski, 2023). If the CO_2 uptake at the two temperatures is compared, an exothermic behavior is deduced since the increase in the temperature led to a decrease in the CO_2 uptake. The Freundlich constant (K_F) decreased with the temperature due to the exothermic nature; and the exponent was higher than the unit in all the cases, which is characteristic of a physisorption process (Haghseresht and Lu, 1998). The efficiency in terms of CO_2 uptake followed the order Cellulose-AC > Acacia-AC ~ Pine-AC > OS-AC > SRF-AC. According to the pore size distribution, all the samples depicted the same HK profile, with no difference among the micropore size most abundant (0.5–0.7 nm). The differences among the samples may be originated from the micropore volume and the presence of oxygenated functional groups able to capture CO_2 molecules. The presence of oxygenated groups, specifically carboxyl and hydroxyl, plays an important role in promoting the adsorption performance due to the predominantly interaction by electrostatic interaction (Song et al., 2020; Jia et al., 2023). According to the characterization by XPS, those materials with the highest CO_2 uptake displayed an important presence of carboxylic groups in the C_{1s} spectra.

Similar CO_2 capacities at room temperature (25 °C) have been reported in the literature with chars activated with KOH (Jung et al., 2019), although the comparison should be taken with caution since the experimental procedure of the activated carbon may vary on the activation temperature or the KOH-char ratio. Olive stone has been the most widely biochar studied to date, with CO_2 uptakes of 88 mg g^{-1} (Plaza et al., 2014), 110 mg g^{-1} (González et al., 2013), and 123 mg g^{-1} (Moussa et al., 2017). In the case of pine, pyrolyzed slash pine led to a CO_2 uptake of 136 mg g^{-1} (Ahmed et al., 2019). For pine, also a higher value has been reported, i.e. 220 mg g^{-1}, over twice the obtained in this work (91 mg g^{-1}), probably due to the higher micropore volume achieved as a consequence of the KOH-char ratio (2:1), higher than the used in this work (1:1) (Deng et al., 2014).

The isosteric heat of adsorption was estimated with the Clausius-Clapeyron equation, and the results are illustrated in Fig. 4B. This figure shows that all the activated chars defined a decreasing isosteric heat of adsorption with the coverage degree of adsorbed CO_2. This common response is associated with the heterogeneity of the surface that entails a preferable linkage to certain active sites, leading to higher exothermicity than the rest. This response is a direct consequence of the good fitting to the Freundlich model, which considers that the adsorption energy logarithmically decreases with the degree of coverage of active sites (Serafin and Dziejarski, 2023). Considering a coverage of 100 mg CO_2 g^{-1} the obtained values are within 18.7–21.5 kJ mol^{-1}. Since values below 40 kJ mol^{-1} are considered physisorption, and values over 80 kJ mol^{-1} are considered strong enough to be chemisorption (Saleh, 2022), the adsorption CO_2 process with the activated char takes place via physisorption. All the samples displayed a very similar profile for the isosteric heat, except for OS-char which defined a curve moved to higher values, but still at low values and considered as physisorption. The commercial-AC performed the weakest interaction with CO_2 molecules.

Regarding the selectivity of the process in CO_2–N_2 mixtures, as displayed in Table 4, the values are within 10–17, Acacia-AC > SRF-AC > Pine-AC > Cellulose-AC > OS-AC. The values obtained among the samples are quite similar in the same order of magnitude.

The CO_2 adsorption onto the chars before and after activation was also assessed by thermogravimetric analysis, see Fig. 5A. The non-activated char performed a moderate CO_2 uptake, within 13.3 mg g^{-1} (SRF-char) and 44.1 mg g^{-1} (OS-char). After activation, the adsorbed CO_2 uptake was increased 2–3 times, depending on the material, giving CO_2 uptakes between 76.8 mg g^{-1} (SRF-AC) and 129.8 mg g^{-1} (Cellulose-AC). These values are slightly lower than the obtained in the physisorption isotherms for the pressure of ~1 bar, probably due to the gas diffusional limitations inside the crucible during the assay carried out in the thermobalance if compared to a gas pycnometer device as used for the construction of the CO_2 isotherm (Dral and ten Elshof, 2018; Babinski et al., 2018). Furthermore, the lack of vacuum in the analysis, and the plausible adsorption of N_2, although limited due to the high selectivity to CO_2, may contribute to further explain the differences.

As shown in Fig. 5A, the CO_2 adsorption kinetics described a rapid process in a short time with no induction period. The kinetics of the process were studied by fitting the temporal data to pseudo-empirical models (Wang and Guo, 2020). Due to the physisorption nature of the process (Ammendola et al., 2017; Singh and Anil Kumar, 2016), Lagergren's pseudo-first order and the fractal Avrami version were those which best described the experimental data, see results in Table 5. The Avrami model slightly improved the fitting values of R^2. The rate constants of all the chars were within 0.20–0.25 min^{-1} either before or after activation. These values are similar to the already reported for the

Table 4
Freundlich parameters of CO_2 adsorption, CO_2/N_2 selectivity at 25 °C, and isosteric adsorption heat.

Sample	T (°C)	Freundlich isotherm $q_{CO_2} = K_F p^{1/n_F}$			q_{CO2} (mg g^{-1}) at 1 bar	CO_2/N_2 Selectivity[b] (%)	$-\Delta H_{ads}$[c] (kJ mol^{-1})
		K_F[a]	n_F	R^2			
OS-AC	0	15.64	1.901	0.994	176.3	13.5	21.5
	25	7.04	1.628	0.997	119.1		
Pine-AC	0	14.79	1.828	0.997	183.7	13.3	18.7
	25	7.98	1.672	0.998	125.4		
Acacia-AC	0	12.35	1.688	0.998	189.0	11.1	20.0
	25	6.01	1.501	0.998	129.2		
SRF-AC	0	10.36	1.663	0.997	165.2	22.7	19.4
	25	5.03	1.508	0.998	106.6		
Cellulose-AC	0	15.07	1.747	0.997	210.3	25.6	19.8
	25	7.51	1.554	0.998	145.4		
Commercial-AC	0	12.23	1.977	0.997	125.6	1.3	12.6
	25	5.40	1.682	0.998	83.4		

[a] K_F in mg g^{-1} kPa^{-nF}.
[b] Selectivity obtained at 25 °C.
[c] Isosteric adsorption heat at $q_{CO2} = 100$ mg g^{-1}.

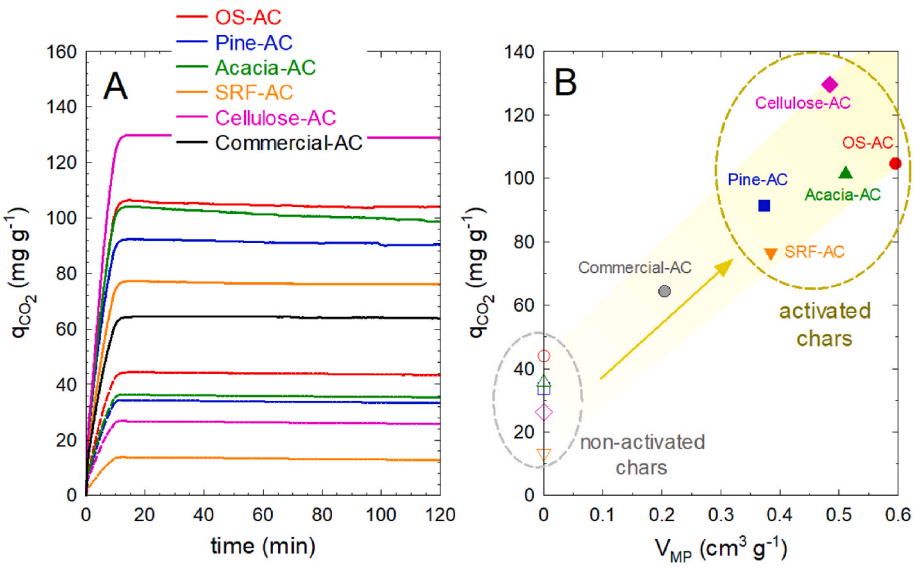

Fig. 5. (A) Temporal evolution of adsorbed CO_2 with the industrial chars before (dashed line) and after activation (solid line). (B) Relationship between the CO_2 uptake (thermobalance) and the microporous volume.

Table 5
Kinetic model parameters of CO_2 adsorption with the industrial chars before and after activation.

Sample	Pseudo-first order			Avrami			
	$q_{CO_2} = q_1(1 - e^{-k_1 t})$			$q_{CO_2} = q_A(1 - e^{-(k_A t)^{n_A}})$			
	q_1 (mg g^{-1})	k_1 (min^{-1})	R^2	q_A (mg g^{-1})	k_A (min^{-1})	n_A	R^2
OS-char	44.1	0.228	0.978	44.0	0.215	1.266	0.988
Pine-char	33.9	0.239	0.973	33.8	0.225	1.274	0.984
Acacia-char	35.9	0.243	0.975	35.8	0.230	1.226	0.983
SRF-char	13.3	0.247	0.944	13.3	0.227	1.339	0.960
Cellulose-char	26.4	0.251	0.970	26.3	0.238	1.203	0.977
OS-AC	104.9	0.231	0.976	104.8	0.218	1.242	0.984
Pine-AC	91.5	0.247	0.979	91.4	0.238	1.149	0.983
Acacia-AC	101.6	0.246	0.964	101.4	0.231	1.241	0.973
SRF-AC	76.7	0.230	0.979	76.6	0.219	1.213	0.986
Cellulose-AC	129.8	0.213	0.978	129.5	0.201	1.315	0.990
Commercial-AC	64.5	0.227	0.985	64.4	0.220	1.158	0.989

q_1 and q_A (mg g^{-1}) are the adsorption at saturation conditions; k_1 (min^{-1}) and k_A (min^{-1}) are the pseudo-first order and Avrami rate constants.

adsorption of CO_2 onto carbonaceous microporous materials, whose pseudo-first order kinetic values range 0.10–0.30 min^{-1} (Díez et al., 2015; Yaumi et al., 2018; Wei et al., 2017; Liu et al., 2014). That suggests a lack of influence of the microporosity developed onto the kinetics of the process, affecting only the saturation value, i.e. the thermodynamics.

The improved adsorption performance after activation can be explained based on the textural properties created. The adsorption efficiency of CO_2 has been strongly correlated to the microporosity developed in the material (Hong et al., 2016; Acevedo et al., 2020) although it depends also on the nature of the functional groups present on the surface (Shafeeyan et al., 2010). It has been reported that activated carbons enriched with micropores, especially pores with diameters inferior to 1 nm were found to show a high CO_2 uptake (Dziejarski et al., 2023). The presence of micropores favors the diffusion of CO_2 in the materials, improving the kinetics of the process (Zhang et al., 2015). Fig. 5B shows the relationship between the CO_2 uptake and the micropore volume, reflecting a proportional effect between the two variables. The sample with the lowest CO_2 uptake, that is the SRF-AC, also led to the less developed microporosity percentage, 71%, whereas the rest of the chars displayed around 90%. The commercial-AC also follows the relationship between CO_2 uptake and the microporosity, with only a ~64 mg g^{-1} of CO_2 were captured due to the low ~33% of micropores present in the sample.

The greater performance of activated carbons has not only been attributed to textural properties such as the presence of larger micropore volume and the presence of narrow micropores but also to the chemistry of the surface, i.e. the presence of oxygenated functional groups (Boujibar et al., 2021). Although Fig. 5B suggests a certain correlation between the CO_2 uptake and the number of micropores, especially when comparing the chars before and after activation, it does not fully explain why Cellulose-AC outstands from the rest, because the micropore volume is slightly higher in the case of Acacia-AC and OS-AC, which provided less adsorption capacity towards CO_2. For that reason, it was studied a plausible relationship between the oxygenated groups on the surface and the CO_2 uptake. Fig. 6 illustrates this relationship considering the amount of C_{XPS} that is linked to oxygen as calculated from the C_{1s} region (see C_{XPS}-Ox column in Table 3). As appreciated in this figure, there is a good linear correlation between the two variables ($R^2 = 0.97$), explaining the CO_2 uptake among the samples. Therefore, it is proved that, besides the microporosity developed, the presence of oxygenated carbon groups also plays a crucial role in the CO_2 uptake. This fact has been reported in the literature previously, in which the raise of oxygenated groups in carbon materials has been objective to enhance

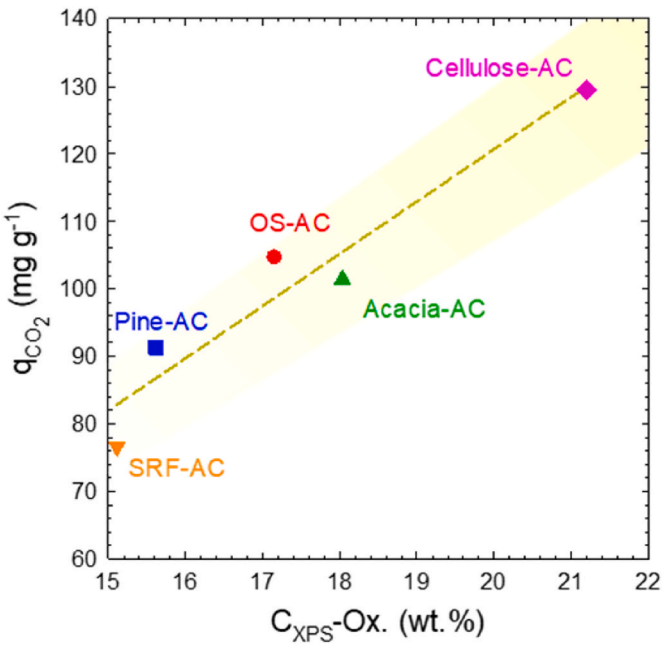

Fig. 6. Relationship between the CO_2 uptake (thermobalance) and the amount of superficial carbon accounting for oxygenated groups (C_{XPS}-Ox).

the efficiency of the material (Giraldo et al., 2020). For instance, the modification of commercial coconut shell-activated carbon aimed at the raise of oxygenated groups has been demonstrated to be efficient in raising the CO_2 uptake, suggesting that the process entails the adsorption within the pores and adsorption onto the oxygen-containing functional groups (Song et al., 2020).

3.3. Adsorption of aqueous heavy metals in water

The activated chars were also tested for the removal of heavy metals, i.e. Pb^{2+}, Zn^{2+}, Ni^{2+}, Cd^{2+}, and Cu^{2+}. The experimental data were fitted to diverse models available in the literature (Mozaffari Majd et al., 2022), such as the classic models of two-parameters, i.e. Freundlich (1907) and Langmuir (1918), or the three-parameter models such as the of Sips (1948), which provided the best adjustment.

The adsorption isotherms are illustrated in Fig. 7 In general terms, comparing the adsorption uptake, regarding the metal the order observed was $Pb^{2+}>Cu^{2+}>Ni^{2+}>Zn^{2+}>Cd^{2+}$. It should be highlighted that in the case of Ni^{2+}, the saturation plateau was not reached. If the different activated chars are compared, it can be stated in general terms that the efficiency followed de order Pine-AC > Acacia-AC > SRF-AC > Cellulose-AC > OS-AC. The adsorption isotherms were fitted to diverse models, giving a better fitting of the three-parameter models, such as the Sips (see results in Table 6), than the two-parameter models of Langmuir or Freundlich. Except for Ni^{2+}, the adsorption reaches a stable plateau and the saturation adsorption uptake could be obtained. For Ni^{2+}, the Sips model extrapolates outside the experimental conditions tested. The adsorption of heavy metals takes place over the mesopores (Kadirvelu et al., 2000). This may explain why the char with the lowest microporosity proportion gave the highest metal adsorption uptake regardless of the type of metal. The presence of mesopores is important but not the only requirement for good adsorption performance. The mechanism of adsorption of metals takes place by electrostatic interaction, ion exchange between metal cations and H^+ ions present in acidic groups, and interaction with the oxygenated surface groups, mainly (Mariana et al., 2021).

In general terms, the metal uptake was lower than the reported values available in the literature (Mariana et al., 2021). There are numerous examples of biochars with higher adsorption uptake of diverse metals before than after chemical activation (Gęca et al., 2022). The development of microporosity and modification of the functional

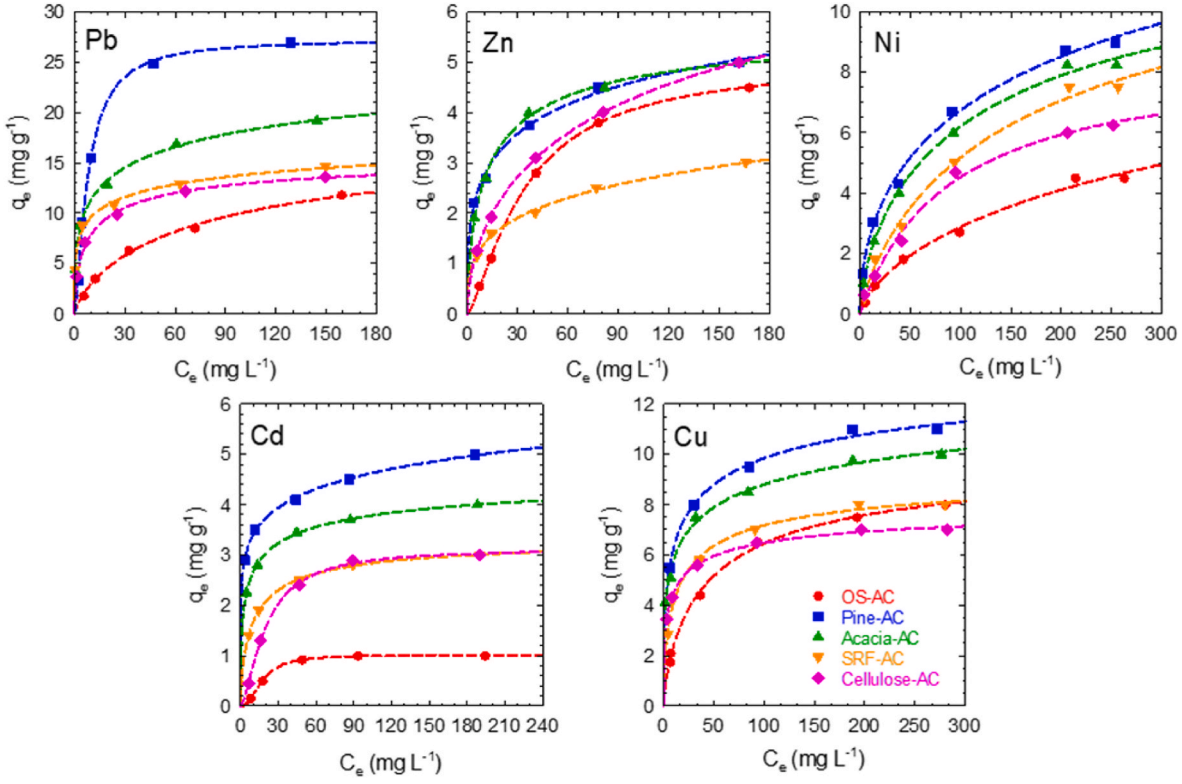

Fig. 7. Metal adsorption isotherms with the activated chars. The dashed lines represent the fitting to the Sips model. *Experimental conditions:* $C_{metal,o}$=5–300 mg L^{-1}; $C_{adsorbent}$=2.0 g L^{-1}; *T=20 °C.*

Table 6
Fitting parameters of metal isotherms to the Sips model.

Metal	Sips parameters	Activated char				
		OS-AC	Pine-AC	Acacia-AC	SRF-AC	Cellulose-AC
Pb^{2+}	q_S	18.91	27.31	23.46	23.58	16.34
	K_S	$1.16{\cdot}10^{-2}$	$1.24{\cdot}10^{-1}$	$1.60{\cdot}10^{-2}$	$2.99{\cdot}10^{-2}$	$8.88{\cdot}10^{-2}$
	n_S	0.782	1.394	0.363	0.310	0.607
	R^2	0.996	0.992	0.996	0.994	0.994
Zn^{2+}	q_S	5.02	11.02	5.89	12.24	10.01
	K_S	$2.88{\cdot}10^{-2}$	$3.77{\cdot}10^{-3}$	$7.54{\cdot}10^{-2}$	$2.06{\cdot}10^{-4}$	$6.15{\cdot}10^{-3}$
	n_S	1.375	0.335	0.678	0.333	0.583
	R^2	0.999	0.994	0.998	0.995	0.999
Ni^{2+}	q_S	12.51	20.47	14.05	13.48	8.64
	K_S	$1.84{\cdot}10^{-3}$	$2.67{\cdot}10^{-3}$	$7.15{\cdot}10^{-3}$	$5.63{\cdot}10^{-3}$	$1.10{\cdot}10^{-2}$
	n_S	0.715	0.539	0.696	0.823	0.994
	R^2	0.992	0.995	0.997	0.993	0.991
Cd^{2+}	q_S	1.01	21.70	4.94	3.40	3.13
	K_S	$5.75{\cdot}10^{-2}$	$2.95{\cdot}10^{-6}$	$1.43{\cdot}10^{-1}$	$9.63{\cdot}10^{-2}$	$5.01{\cdot}10^{-2}$
	n_S	2.259	0.161	0.440	0.703	1.504
	R^2	0.999	0.998	0.999	0.999	0.998
Cu^{2+}	q_S	10.10	15.11	15.90	9.51	8.46
	K_S	$2.10{\cdot}10^{-2}$	$4.39{\cdot}10^{-2}$	$1.90{\cdot}10^{-2}$	$6.34{\cdot}10^{-2}$	$1.31{\cdot}10^{-1}$
	n_S	0.762	0.422	0.334	0.605	0.131
	R^2	0.998	0.994	0.993	0.993	0.459

q_e (mg g^{-1}) refers to the amount of adsorbed metal at equilibrium; C_e (mg L^{-1}) is the solute concentration at equilibrium; q_S (mg g^{-1}) is the adsorption capacity of Sips model; K_S (L mg^{-1}) is the Sips constant; and n_S (dimensionless) means the exponent of the Sips model.

groups of the surface may result in the detriment of the adsorption performance. The presence of mesoporosity and high electrostatic charge results in decisive efficiency (Chen and Lin, 2001). The use of apricot stone after activation with H_2SO_4 has reported a Pb uptake of 21.4 mg g^{-1} (Kadirvelu et al., 2000), close to the 27 registered by Pine AC. Apple pulp was activated with $ZnCl_2$ and capable of capturing 10.5 mg g^{-1} of Pb^{2+} and 9.3 mg g^{-1} of Zn^{2+} (Gęca et al., 2022).

3.4. Adsorption of aqueous contaminants of emerging concern

The adsorption of contaminants of emerging concern onto the activated chars was evaluated by selecting three organic contaminants of emerging concern due to their high occurrence in wastewater, such as acetaminophen, caffeine, and diclofenac. The adsorption isotherms are plotted in Fig. 8. In many cases a stable value plateau was reached, enabling the estimation of the saturation capacity. Among the vast number of isotherms models available in the literature (Mozaffari Majd et al., 2022), the data was fitted to the classic models such as the two-parameter Freundlich (1907) and Langmuir (1918) and the three-parameter model of Sips (1948). The best fitting was achieved with the Sips model (see Table 7), probably due to its hybrid character, suitable for the prediction of the adsorption behavior of the heterogeneous surface, and avoiding the restriction of the increasing concentration of adsorbate that Freundlich isotherm supposes (Mozaffari Majd et al., 2022). Fig. 8 depicts the high adsorption capacity of the activated materials. There are no observed great differences among the contaminants tested in the saturation adsorption uptake if visually compared in Fig. 8, being the saturation uptake in all the materials with the three selected pollutants within roughly 200–500 mg g^{-1}, according to the experimental interval of conditions studied. It is observed the same behavior when comparing the adsorbents with the three pollutants. The Pine-AC displayed less saturation uptake, i.e. 200-250 mg g^{-1} in the interval of C_e studied. The activated char most active was OS-AC, with a performance of briefly 400–500 mg g^{-1}. The other three activated char, i.e. Acacia-AC, SRF-AC, and Cellulose-AC, described intermediate adsorption uptakes, with isotherms profiles very similar among them in the case of CAF and DCF, and more differentiated with ACE. The adsorption mechanism of CECs onto activated carbon materials involves hydrogen bonding, hydrophobic, and electrostatic interactions between the adsorbate molecule and the surface of the activated material (Sophia A and Lima, 2018). The sample OS-char, which performed the highest surface area and a moderate presence of oxygenated groups, led to the

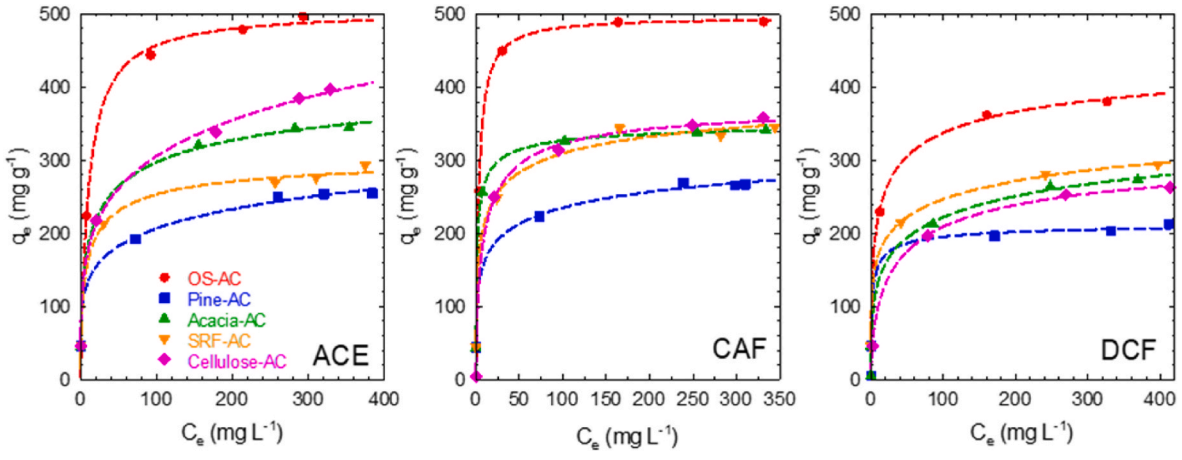

Fig. 8. Adsorption isotherms with the activated chars with acetaminophen (ACE), caffeine (CAF), and diclofenac (DCF). The dashed lines represent the fitting to the Sips model. *Experimental conditions:* $C_{CEC,0}$=*10*–500 mg L^{-1}; $C_{adsorbent}$=*0.4-2.0* g L^{-1}; *T=20 °C.*

Table 7
Fitting parameters of CECs isotherms to the Sips model.

CEC	Sips parameters	Activated char				
		OS-AC	Pine-AC	Acacia-AC	SRF-AC	Cellulose-AC
ACE	q_S	506.05	956.29	459.90	314.53	1328.41
	K_S	$1.02{\cdot}10^{-1}$	$3.35{\cdot}10^{-5}$	$3.99{\cdot}10^{-2}$	$1.13{\cdot}10^{-1}$	$1.48{\cdot}10^{-4}$
	n_S	0.966	0.226	0.437	0.588	0.287
	R^2	0.998	0.997	0.999	0.996	0.999
CAF	q_S	496.24	421.61	356.84	433.54	381.51
	K_S	$3.24{\cdot}10^{-1}$	$2.14{\cdot}10^{-2}$	$7.35{\cdot}10^{-1}$	$9.73{\cdot}10^{-2}$	$1.14{\cdot}10^{-1}$
	n_S	1.005	0.305	0.557	0.402	0.699
	R^2	0.999	0.998	0.999	0.994	0.999
DCF	q_S	482.35	217.77	471.76	559.98	330.76
	K_S	$7.00{\cdot}10^{-2}$	$5.43{\cdot}10^{-1}$	$7.19{\cdot}10^{-3}$	$3.97{\cdot}10^{-3}$	$2.46{\cdot}10^{-2}$
	n_S	0.435	0.544	0.350	0.258	0.602
	R^2	0.996	0.997	0.997	0.999	0.999

q_e (mg g^{-1}) refers to the amount of meal adsorbed at equilibrium; C_e (mg L^{-1}) is the solute concentration at equilibrium; q_S (mg g^{-1}) is the adsorption capacity of Sips model; K_S (L mg^{-1}) is the Sips constant; and n_S (dimensionless) means the exponent of the Sips model.

highest CECs uptake which suggests that well-developed textural properties are decisive for the CECs retention.

The sample OS-char performed the highest value of contaminant uptake at saturation conditions within the interval of equilibria concentration studied. This value is very competitive if compared to the reported values in the literature for similar biochar precursors activated with KOH. For instance, using durian seed it has been reported a maximum ACE adsorption capacity of 304 mg g^{-1} (Foo, 2018) or 330 mg g^{-1} after activation of Jatoba bark (Spessato et al., 2019). A value in the same order as the OS-AC of this work has been reported with tree Bark residues, 571 mg g^{-1} (dos Reis et al., 2022). This work also demonstrated that KOH displayed as an activating agent better textural properties and adsorption ability than $ZnCl_2$ (411 mg g^{-1}), $ZnSO_4$ (363 mg g^{-1}), and $MgCl_2$ (222 mg g^{-1}) (dos Reis et al., 2022). Other activated carbons prepared with different chemical agents have provided good adsorption capacities, such 118 mg g^{-1} using as precursor orange peels with (activation with $ZnCl_2$) (El Saied et al., 2022), 300 mg g^{-1} with lignin (activation with $FeCl_3$) (Gómez-Avilés et al., 2021), 200 mg g^{-1} with cork powder (activation with K_2CO_3) (Cabrita et al., 2010), 435 mg g^{-1} with pine wood (activation with K_2CO_3) (Galhetas et al., 2014), 204 mg g^{-1} with peach stones (activation with K_2CO_3) (Cabrita et al., 2010) or 113 mg g^{-1} with polyethylene terephthalate (activation with K_2CO_3) (Cabrita et al., 2010). A commercial formula has reported a saturation capacity of 245 mg g^{-1} (Filtrasorb-400 from Chemvron) (Lladó et al., 2015), 117 mg g^{-1} (Norit PK 1–3) (Lladó et al., 2015) or 221 mg g^{-1} (Nguyen et al., 2020). All the activated chars prepared in this study improved the adsorption uptake of these commercial formula.

Regarding the maximum uptake reached for CAF, 496 mg g^{-1}, with OS-AC. Spent coffee capsules were activated with KOH and led to a CAF maximum uptake of 315 mg g^{-1} (Mengesha et al., 2022). Plastic waste activated with KOH has reported 351 mg g^{-1} of CAF saturation capacity (Sarici-Özdemir and Önal, 2016). Regarding alternative activating agents, K_2CO_3 with pine wood led to 500 mg g^{-1} (Galhetas et al., 2014), 177 mg g^{-1} using açaí seed activated with K_2CO_3 (Da Silva Vasconcelos De Almeida et al., 2021), 296 mg g^{-1} with residue from the biofuel production after treatment with K_2CO_3 (Batista et al., 2016), 260–270 mg g^{-1} for peach stones activated with H_3PO_4 (Torrellas et al., 2015), 367 mg g^{-1} with grape stalks after H_3PO_4 activation (Portinho et al., 2017), pineapple leaves where activated with H_3PO_4 and led to 155 mg g^{-1} (Beltrame et al., 2018), or 118 mg g^{-1} with macrophytes plants activated with CO_2 (Zanella et al., 2021). Commercial formulas have provided maximum CAF uptakes of 270 mg g^{-1} (Calgon Filtrasorb 400) (Sotelo et al., 2012).

In the case of DCF, the maximum uptake of the OS-AC is estimated, according to Fig. 9, almost 500 mg g^{-1}. This value is very competitive if compared to other activated carbonaceous materials prepared from biochars which usually provide low DCF uptakes (Ighalo and Adeniyi, 2020). Some exceptions are the use of sugar cane bagasse activated with $ZnCl_2$ which displayed a DCF uptake of 315 mg g^{-1} (Abo El Naga et al., 2019), the activation of Sycamore balls with $ZnCl_2$ and uptake of 179 mg g^{-1} (Avcu et al., 2021), or the activation of sunflower seed with H_3PO_4 which reported an extraordinarily high DCF maximum uptake of 690 mg g^{-1}, attributed to the surface -P_2O_7, and –COOH groups and acidity (Alvear-Daza et al., 2022). A study using tea waste as carbon precursor, and different chemical agents for the activation led to DCF adsorption capacities below 100 mg g^{-1}, i.e. 81 mg g^{-1} ($ZnCl_2$), 82 mg g^{-1} (K_2CO_3), and 75 mg g^{-1} (KOH) (Malhotra et al., 2018). Commercial formulas have provided much lower DCF uptake than any of the prepared activated carbon. For instance, WG-12 (Gryfskand, Poland), F-300 (Chemviron Carbon), and ROW 08 Supra (Norit) have led to DCF uptakes of, respectively, 89 mg g^{-1}, 108 mg g^{-1} and 90 mg g^{-1} (Lach and Szymonik, 2018).

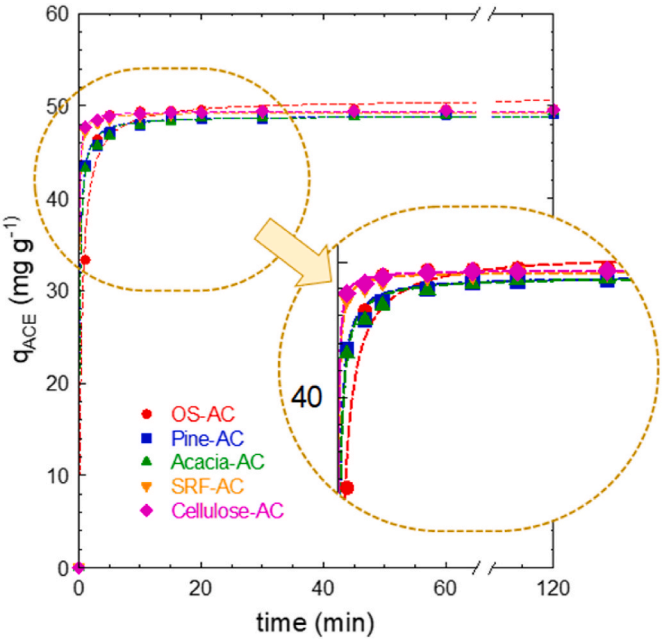

Fig. 9. Kinetic adsorption of ACE onto the activated chars. The dashed lines represent the fittings to the pseudo-second order model. *Experimental conditions:* $C_{ACE,0}$=100 mg L^{-1}; $C_{adsorbent}$=2.0 g L^{-1}; *T=25 °C.*

The kinetics of the adsorption process of the CECs over the activated chars was studied due to the paramount importance of selecting the retention time at real scale-up applications. As the adsorption behavior of the three selected CECs was very similar to the activated chars, ACE

was selected for the study of the kinetics of the process, aimed at the comparison among the materials rather than the behavior with other contaminants. Fig. 9 illustrates the temporal evolution of the ACE uptake over the five activated chars. As observed, the adsorption process of ACE is very fast, reaching the maximum adsorption capacity of roughly 10 min. Noteworthily, it should be mentioned that the sample at 120 min did not display any detectable peak in the HPLC. The kinetics of the process were modeled to diverse models, such as Lagergren's pseudo-first order, Ho's pseudo-second order, intraparticle diffusion, or Elovich's diffusional model (Wang et al., 2022b; Stevens et al., 2013). It was the pseudo-second order that led to the best fitting of the experimental data. The results are shown in Table 8. The driving force assumed by the pseudo-second order model provided the best fitting. The comparison of the k_2-values confirmed that the kinetics was faster according to the order Cellulose-AC > SRF-AC > Pine-AC ~ Acacia-AC > OS-AC. This kinetic constant value, although affected by diffusional effects related to the design of the crucible, was compared to the reported in the literature. The Cellulose-AC displayed a second-order rate constant, $k_2 = 5.127{\cdot}10^{-1}$ mg^{-1} g min^{-1}, a high value if compared to the reported in the literature. Similar kinetics have been described with commercial formulas of activated carbon (Ruiz et al., 2010) or considerably faster than other carbonaceous materials under research such as activated carbon prepared from the activation of lignin char with $FeCl_3$ (Gómez-Avilés et al., 2021; Sellaoui et al., 2023).

4. Conclusions

The activation of chars obtained from agroforestry and industrial activities possess interesting properties that make them good candidates for the preparation of activated carbons. Thus, it is given a solution for a residue currently produced in diverse pyrolysis factories. The valorization of this carbon-enriched residue through chemical activation led to the production of highly microporous materials which display diverse potential applications in the depuration of gas and liquid effluents.

Considering the adsorption of CO_2, the overall adsorption uptake was explained in terms of the microporosity developed after the activation with KOH, which led to carbonaceous solids in which over 80% of the pore volume accounts as micropore (most frequent size around 0.5 nm). Not only does the presence of narrow micropores enhance the performance of CO_2 adsorption, but also the surface chemistry, i.e. the oxygen-containing function, which explains the adsorption performance among the activated chars. The higher the content of oxygenated groups, the larger the CO_2 uptake.

Regarding the efficiency of the adsorption of heavy metals, it was observed a moderate adsorption capacity, due to the limited presence of mesopores. Hence, the best performance was recorded for the removal of Pb, saturation uptake ~20 mg g^{-1}. Better results were achieved in the adsorption of organic contaminants of emerging concern, i.e. acetaminophen, caffeine, and diclofenac. Depending on the nature of the char activated the contaminant uptake was within 200–500 mg g^{-1}, which makes them very competitive for a real application. More interestingly, the kinetics of the process was described as a pseudo-second order process with fast kinetics which enables them for a real practical alternative.

As a future outlook, further investigation of the activation process at a larger scale close to industrial production should be conducted, validating the results already obtained at a lab scale. Moreover, detailed research should be conducted to address the regeneration of the spent adsorbent after submitted to an aqueous application.

CRediT authorship contribution statement

Ledicia Pereira: Formal analysis, Investigation, Methodology. **Ventura Castillo:** Investigation, Methodology, Writing – original draft. **Mónica Calero:** Funding acquisition, Investigation, Project administration, Resources, Writing – review & editing. **Sergio González-Egido:** Funding acquisition, Resources. **M. Ángeles Martín-Lara:** Formal analysis, Funding acquisition, Investigation, Supervision, Writing – review & editing. **Rafael R. Solís:** Formal analysis, Investigation, Methodology, Supervision, Writing – original draft, Writing – review & editing.

Table 8
Adsorption kinetics of ACE with the activated chars. The dashed lines represent the fittings to the pseudo-second order model. *Experimental conditions as shown in* Fig. 9.

Sample	$q_{ACE} = \frac{k_2 q_2^2 t}{1 + k_2 q_2 t}$		
	q_2	$k_2{\cdot}10^2$	R^2
OS-AC	50.7	4.53	0.992
Pine-AC	48.9	14.96	0.982
Acacia-AC	48.9	13.97	0.999
SRF-AC	49.3	42.50	0.999
Cellulose-AC	49.4	51.27	0.999

q_2 (mg g^{-1}) refers to the amount of ACE adsorbed at equilibrium; k_2 (mg^{-1} g min^{-1}) is the Sips constant, and n_S (dimensionless) means the exponent of the Sips model.

Declaration of competing interest

The authors declare that they have no known competing financial interests or personal relationships that could have appeared to influence the work reported in this paper.

Data availability

Data will be made available on request.

Acknowledgments

Grant CPP 2021-008551 funded by MICIU/AEI/10.13039/501100011033, and, as appropriate, by "ERDF a way of making Europe", by "ERDF/EU", by the "European Union NextGenerationEU/PRTR". They also thank the support provided for the external services of investigation of the University of Granada ("Centro de Instrumentación Científica", CIC). Finally, the authors also are thankful to "Neoliquid Advanced Biofuels and Biochemicals S.L." for providing the industrial chars from municipal solid waste, "Grupo Layna Gestión de Residuos S. L." for providing the industrial char from biomass waste, and "Ecocuadrado S.L." for providing municipal and industrial solid waste. Funding for open access charge: Universidad de Granada/CBUA.

References

Abo El Naga, A.O., El Saied, M., Shaban, S.A., El Kady, F.Y., 2019. Fast removal of diclofenac sodium from aqueous solution using sugar cane bagasse-derived activated carbon. J. Mol. Liq. 285, 9–19. https://doi.org/10.1016/J.MOLLIQ.2019.04.062.

Acevedo, S., Giraldo, L., Moreno-Piraján, J.C., 2020. Adsorption of CO_2 on activated carbons prepared by chemical activation with cupric nitrate. ACS Omega 5, 10423–10432. https://doi.org/10.1021/ACSOMEGA.0C00342.

Ahmed, A., Abu Bakar, M.S., Azad, A.K., Sukri, R.S., Phusunti, N., 2018. Intermediate pyrolysis of Acacia cincinnata and Acacia holosericea species for bio-oil and biochar production. Energy Convers. Manag. 176, 393–408. https://doi.org/10.1016/J.ENCONMAN.2018.09.041.

Ahmed, M.B., Hasan Johir, M.A., Zhou, J.L., Ngo, H.H., Nghiem, L.D., Richardson, C., Moni, M.A., Bryant, M.R., 2019. Activated carbon preparation from biomass feedstock: clean production and carbon dioxide adsorption. J. Clean. Prod. 225, 405–413. https://doi.org/10.1016/J.JCLEPRO.2019.03.342.

Akeeb, O., Wang, L., Xie, W., Davis, R., Alkasrawi, M., Toan, S., 2022. Post-combustion CO_2 capture via a variety of temperature ranges and material adsorption process: a review. J. Environ. Manag. 313, 115026 https://doi.org/10.1016/J.JENVMAN.2022.115026.

Alothman, Z.A., 2012. A review: fundamental aspects of silicate mesoporous materials. Materials 5, 2874–2902. https://doi.org/10.3390/MA5122874.

Alvear-Daza, J.J., Cánneva, A., Donadelli, J.A., Manrique-Holguín, M., Rengifo-Herrera, J.A., Pizzio, L.R., 2022. Removal of diclofenac and ibuprofen on mesoporous activated carbon from agro-industrial wastes prepared by optimized

synthesis employing a central composite design. Biomass Convers Biorefin 1, 1–23. https://doi.org/10.1007/S13399-021-02227-W/TABLES/10.
Ammendola, P., Raganati, F., Chirone, R., 2017. CO_2 adsorption on a fine activated carbon in a sound assisted fluidized bed: thermodynamics and kinetics. Chem. Eng. J. 322, 302–313. https://doi.org/10.1016/J.CEJ.2017.04.037.
Avcu, T., Üner, O., Geçgel, Ü., 2021. Adsorptive removal of diclofenac sodium from aqueous solution onto sycamore ball activated carbon – isotherms, kinetics, and thermodynamic study. Surface. Interfac. 24, 101097 https://doi.org/10.1016/J.SURFIN.2021.101097.
Avrami, M., 1939. Kinetics of phase change. I general theory. J. Chem. Phys. 7, 1103–1112. https://doi.org/10.1063/1.1750380.
Babinski, P., Sciazko, M., Ksepko, E., 2018. Limitation of thermogravimetry for oxy-combustion analysis of coal chars. J. Therm. Anal. Calorim. 133, 713–725. https://doi.org/10.1007/S10973-017-6782-6/FIGURES/7.
Baby, R., Saifullah, B., Hussein, M.Z., 2019. Carbon nanomaterials for the treatment of heavy metal-contaminated water and environmental remediation. Nanoscale Res. Lett. 14 (1 14), 1–17. https://doi.org/10.1186/S11671-019-3167-8, 2019.
Batista, M.K.S., Mestre, A.S., Matos, I., Fonseca, I.M., Carvalho, A.P., 2016. Biodiesel production waste as promising biomass precursor of reusable activated carbons for caffeine removal. RSC Adv. 6, 45419–45427. https://doi.org/10.1039/C6RA09006K.
Beltrame, K.K., Cazetta, A.L., de Souza, P.S.C., Spessato, L., Silva, T.L., Almeida, V.C., 2018. Adsorption of caffeine on mesoporous activated carbon fibers prepared from pineapple plant leaves. Ecotoxicol. Environ. Saf. 147, 64–71. https://doi.org/10.1016/J.ECOENV.2017.08.034.
Bläker, C., Muthmann, J., Pasel, C., Bathen, D., 2019. Characterization of activated carbon adsorbents – state of the art and novel approaches. ChemBioEng Rev. 6, 119–138. https://doi.org/10.1002/CBEN.201900008.
Boujibar, O., Ghamouss, F., Ghosh, A., Achak, O., Chafik, T., 2021. Efficient CO_2 capture by ultra-high microporous activated carbon made from natural coal. Chem. Eng. Technol. 44, 148–155. https://doi.org/10.1002/CEAT.202000138.
Burg, P., Fydrych, P., Cagniant, D., Nanse, G., Bimer, J., Jankowska, A., 2002. The characterization of nitrogen-enriched activated carbons by IR, XPS and LSER methods. Carbon N Y 40, 1521–1531. https://doi.org/10.1016/S0008-6223(02)00004-0.
Cabrita, I., Ruiz, B., Mestre, A.S., Fonseca, I.M., Carvalho, A.P., Ania, C.O., 2010. Removal of an analgesic using activated carbons prepared from urban and industrial residues. Chem. Eng. J. 163, 249–255. https://doi.org/10.1016/J.CEJ.2010.07.058.
Chen, J.P., Lin, M., 2001. Surface charge and metal ion adsorption on an H-type activated carbon: experimental observation and modeling simulation by the surface complex formation approach. Carbon N Y 39, 1491–1504. https://doi.org/10.1016/S0008-6223(00)00277-3.
Da Silva Vasconcelos De Almeida, A., Vieira, W.T., Bispo, M.D., De Melo, S.F., Da Silva, T.L., Balliano, T.L., Vieira, M.G.A., Soletti, J.I., 2021. Caffeine removal using activated biochar from açaí seed (Euterpe oleracea Mart): experimental study and description of adsorbate properties using Density Functional Theory (DFT). J. Environ. Chem. Eng. 9, 104891 https://doi.org/10.1016/J.JECE.2020.104891.
Deng, S., Wei, H., Chen, T., Wang, B., Huang, J., Yu, G., 2014. Superior CO_2 adsorption on pine nut shell-derived activated carbons and the effective micropores at different temperatures. Chem. Eng. J. 253, 46–54. https://doi.org/10.1016/J.CEJ.2014.04.115.
Díez, N., Álvarez, P., Granda, M., Blanco, C., Santamaría, R., Menéndez, R., 2015. CO_2 adsorption capacity and kinetics in nitrogen-enriched activated carbon fibers prepared by different methods. Chem. Eng. J. 281, 704–712. https://doi.org/10.1016/J.CEJ.2015.06.126.
Dombrowski, R.J., Lastoskie, C.M., Hyduke, D.R., 2001. The Horvath–Kawazoe method revisited. Colloids Surf A Physicochem Eng Asp 187–188 23–39. https://doi.org/10.1016/S0927-7757(01)00618-5.
dos Reis, G.S., Guy, M., Mathieu, M., Jebrane, M., Lima, E.C., Thyrel, M., Dotto, G.L., Larsson, S.H., 2022. A comparative study of chemical treatment by $MgCl_2$, $ZnSO_4$, $ZnCl_2$, and KOH on physicochemical properties and acetaminophen adsorption performance of biobased porous materials from tree bark residues. Colloids Surf. A Physicochem. Eng. Asp. 642, 128626 https://doi.org/10.1016/J.COLSURFA.2022.128626.
Dral, A.P., ten Elshof, J.E., 2018. Analyzing microporosity with vapor thermogravimetry and gas pycnometry. Microporous Mesoporous Mater. 258, 197–204. https://doi.org/10.1016/J.MICROMESO.2017.09.015.
Dziejarski, B., Serafin, J., Andersson, K., Krzyżyńska, R., 2023. CO_2 capture materials: a review of current trends and future challenges. Materials Today Sustainability, 100483. https://doi.org/10.1016/J.MTSUST.2023.100483.
El Saied, M., Shaban, S.A., Mostafa, M.S., El Naga, A.O.A., 2022. Efficient adsorption of acetaminophen from the aqueous phase using low-cost and renewable adsorbent derived from orange peels. Biomass Convers Biorefin 1, 1–18. https://doi.org/10.1007/S13399-022-02541-X.
Fan, M., Li, C., Sun, Y., Zhang, L., Zhang, S., Hu, X., 2021. In situ characterization of functional groups of biochar in pyrolysis of cellulose. Sci. Total Environ. 799, 149354 https://doi.org/10.1016/J.SCITOTENV.2021.149354.
Foo, K.Y., 2018. Preparation of eco-friendly activated carbon as a refining solution for the adsorptive treatment of analgesic acetaminophen. Desalination Water Treat. 118, 332–340. https://doi.org/10.5004/dwt.2018.22354.
Freundlich, H., 1907. Über die Adsorption in Lösungen. Z. Phys. Chem. 57U, 385–470. https://doi.org/10.1515/ZPCH-1907-5723.
Fuller, R., Landrigan, P.J., Balakrishnan, K., Bathan, G., Bose-O'Reilly, S., Brauer, M., Caravanos, J., Chiles, T., Cohen, A., Corra, L., Cropper, M., Ferraro, G., Hanna, J., Hanrahan, D., Hu, H., Hunter, D., Janata, G., Kupka, R., Lanphear, B., Lichtveld, M., Martin, K., Mustapha, A., Sanchez-Triana, E., Sandilya, K., Schaefli, L., Shaw, J., Seddon, J., Suk, W., Téllez-Rojo, M.M., Yan, C., 2022. Pollution and health: a progress update. Lancet Planet. Health 6, e535–e547. https://doi.org/10.1016/S2542-5196(22)00090-0.
Galhetas, M., Mestre, A.S., Pinto, M.L., Gulyurtlu, I., Lopes, H., Carvalho, A.P., 2014. Chars from gasification of coal and pine activated with K_2CO_3: acetaminophen and caffeine adsorption from aqueous solutions. J. Colloid Interface Sci. 433, 94–103. https://doi.org/10.1016/J.JCIS.2014.06.043.
Gao, Y., Yue, Q., Gao, B., Li, A., 2020. Insight into activated carbon from different kinds of chemical activating agents: a review. Sci. Total Environ. 746, 141094 https://doi.org/10.1016/J.SCITOTENV.2020.141094.
García Martín, J.F., Cuevas, M., Feng, C.H., Mateos, P.Á., García, M.T., Sánchez, S., 2020. Energetic valorisation of olive biomass: olive-tree pruning, olive stones and pomaces. Processes 8, 511. https://doi.org/10.3390/PR8050511.
Gauden, P.A., Terzyk, A.P., Rychlicki, G., Kowalczyk, P., Ćwiertnia, M.S., Garbacz, J.K., 2004. Estimating the pore size distribution of activated carbons from adsorption data of different adsorbates by various methods. J. Colloid Interface Sci. 273, 39–63. https://doi.org/10.1016/J.JCIS.2003.08.033.
Gęca, M., Wiśniewska, M., Nowicki, P., 2022. Biochars and activated carbons as adsorbents of inorganic and organic compounds from multicomponent systems – a review. Adv. Colloid Interface Sci. 305, 102687 https://doi.org/10.1016/J.CIS.2022.102687.
Georgin, J., Franco, D.S.P., Schadeck Netto, M., Allasia, D., Foletto, E.L., Oliveira, L.F.S., Dotto, G.L., 2021. Transforming shrub waste into a high-efficiency adsorbent: application of Physalis peruvian chalice treated with strong acid to remove the 2,4-dichlorophenoxyacetic acid herbicide. J. Environ. Chem. Eng. 9, 104574 https://doi.org/10.1016/J.JECE.2020.104574.
Ghanbarpour Mamaghani, Z., Hawboldt, K.A., MacQuarrie, S., 2023. Adsorption of CO_2 using biochar - review of the impact of gas mixtures and water on adsorption. J. Environ. Chem. Eng. 11, 109643 https://doi.org/10.1016/J.JECE.2023.109643.
Gil, M.V., Riaza, J., Álvarez, L., Pevida, C., Rubiera, F., 2015. Biomass devolatilization at high temperature under N_2 and CO_2: char morphology and reactivity. Energy 91, 655–662. https://doi.org/10.1016/J.ENERGY.2015.08.074.
Giraldo, L., Vargas, D.P., Moreno-Piraján, J.C., 2020. Study of CO_2 adsorption on chemically modified activated carbon with nitric acid and ammonium aqueous. Front. Chem. 8, 543452 https://doi.org/10.3389/FCHEM.2020.543452.
Gómez-Avilés, A., Peñas-Garzón, M., Belver, C., Rodriguez, J.J., Bedia, J., 2021. Equilibrium, kinetics and breakthrough curves of acetaminophen adsorption onto activated carbons from microwave-assisted $FeCl_3$-activation of lignin. Sep. Purif. Technol. 278, 119654 https://doi.org/10.1016/J.SEPPUR.2021.119654.
González, A.S., Plaza, M.G., Rubiera, F., Pevida, C., 2013. Sustainable biomass-based carbon adsorbents for post-combustion CO_2 capture. Chem. Eng. J. 230, 456–465. https://doi.org/10.1016/J.CEJ.2013.06.118.
Guo, S., Li, Y., Wang, Y., Wang, L., Sun, Y., Liu, L., 2022. Recent advances in biochar-based adsorbents for CO_2 capture. Carbon Capture Science & Technology 4, 100059. https://doi.org/10.1016/J.CCST.2022.100059.
Haghseresht, F., Lu, G.Q., 1998. Adsorption characteristics of phenolic compounds onto coal-reject-derived adsorbents. Energy Fuel. 12, 1100–1107. https://doi.org/10.1021/EF9801165.
He, S., Chen, G., Xiao, H., Shi, G., Ruan, C., Ma, Y., Dai, H., Yuan, B., Chen, X., Yang, X., 2021. Facile preparation of N-doped activated carbon produced from rice husk for CO_2 capture. J. Colloid Interface Sci. 582, 90–101. https://doi.org/10.1016/J.JCIS.2020.08.021.
Heberer, T., 2002. Tracking persistent pharmaceutical residues from municipal sewage to drinking water. J. Hydrol. (Amst.) 266, 175–189. https://doi.org/10.1016/S0022-1694(02)00165-8.
Ho, Y.S., McKay, G., 1999. Pseudo-second order model for sorption processes. Process Biochem. 34, 451–465. https://doi.org/10.1016/S0032-9592(98)00112-5.
Hong, W.Y., 2022. A techno-economic review on carbon capture, utilisation and storage systems for achieving a net-zero CO_2 emissions future. Carbon Capture Science & Technology 3, 100044. https://doi.org/10.1016/J.CCST.2022.100044.
Hong, S.M., Jang, E., Dysart, A.D., Pol, V.G., Lee, K.B., 2016. CO_2 capture in the sustainable wheat-derived activated microporous carbon compartments. Sci. Rep. 6 (1 6), 1–10. https://doi.org/10.1038/srep34590, 2016.
Huang, J., Rther, T., 2009. Why are ionic liquids attractive for CO_2 absorption? An overview. Aust. J. Chem. 62, 298–308. https://doi.org/10.1071/CH08559.
Huang, L., Shen, R., Shuai, Q., 2021. Adsorptive removal of pharmaceuticals from water using metal-organic frameworks: a review. J. Environ. Manag. 277, 111389 https://doi.org/10.1016/J.JENVMAN.2020.111389.
Huff, M.D., Kumar, S., Lee, J.W., 2014. Comparative analysis of pinewood, peanut shell, and bamboo biomass derived biochars produced via hydrothermal conversion and pyrolysis. J. Environ. Manag. 146, 303–308. https://doi.org/10.1016/J.JENVMAN.2014.07.016.
Ighalo, J.O., Adeniyi, A.G., 2020. Mitigation of diclofenac pollution in aqueous media by adsorption. ChemBioEng Rev. 7, 50–64. https://doi.org/10.1002/CBEN.201900020.
Jia, J., Zhao, H., He, M., Wang, Z., Sun, Z., Yang, X., Yu, Q., Qu, Z., Pi, X., Yao, F., 2023. Investigation of the mechanisms of CO_2/O_2 adsorption selectivity on carbon materials enhanced by oxygen functional groups. Langmuir 39, 14699–14710. https://doi.org/10.1021/ACS.LANGMUIR.3C02076.
jia Liu, S., guo Liu, Y., fei Tan, X., ming Zeng, G., hui Zhou, Y., bo Liu, S., hong Yin, Z., hua Jiang, L., fang Li, M., Wen, J., 2018. The effect of several activated biochars on Cd immobilization and microbial community composition during in-situ remediation of heavy metal contaminated sediment. Chemosphere 208, 655–664. https://doi.org/10.1016/J.CHEMOSPHERE.2018.06.023.
Jung, S., Park, Y.K., Kwon, E.E., 2019. Strategic use of biochar for CO_2 capture and sequestration. J. CO2 Util. 32, 128–139. https://doi.org/10.1016/J.JCOU.2019.04.012.

Kadirvelu, K., Faur-Brasquet, C., Le Cloirec, P., 2000. Removal of Cu(II), Pb(II), and Ni (II) by adsorption onto activated carbon cloths. Langmuir 16, 8404–8409. https://doi.org/10.1021/LA0004810.

Kasonga, T.K., Coetzee, M.A.A., Kamika, I., Ngole-Jeme, V.M., Benteke Momba, M.N., 2021. Endocrine-disruptive chemicals as contaminants of emerging concern in wastewater and surface water: a review. J. Environ. Manag. 277, 111485 https://doi.org/10.1016/J.JENVMAN.2020.111485.

Kaur, B., Gupta, R.K., Bhunia, H., 2019. CO_2 capture on activated carbon from PET (polyethylene terephthalate) waste: kinetics and modeling studies. Chem. Eng. Commun. 207, 1031–1047. https://doi.org/10.1080/00986445.2019.1635466.

Kerkhoff, C.M., da Boit Martinello, K., Franco, D.S.P., Netto, M.S., Georgin, J., Foletto, E. L., Piccilli, D.G.A., Silva, L.F.O., Dotto, G.L., 2021. Adsorption of ketoprofen and paracetamol and treatment of a synthetic mixture by novel porous carbon derived from Butia capitata endocarp. J. Mol. Liq. 339, 117184 https://doi.org/10.1016/J.MOLLIQ.2021.117184.

Kim, K.H., Kim, J.Y., Cho, T.S., Choi, J.W., 2012. Influence of pyrolysis temperature on physicochemical properties of biochar obtained from the fast pyrolysis of pitch pine (Pinus rigida). Bioresour. Technol. 118, 158–162. https://doi.org/10.1016/J.BIORTECH.2012.04.094.

Kozyatnyk, I., Oesterle, P., Wurzer, C., Mašek, O., Jansson, S., 2021. Removal of contaminants of emerging concern from multicomponent systems using carbon dioxide activated biochar from lignocellulosic feedstocks. Bioresour. Technol. 340, 125561 https://doi.org/10.1016/J.BIORTECH.2021.125561.

Kümmerer, K., Dionysiou, D.D., Olsson, O., Fatta-Kassinos, D., 2018. A path to clean water. Science 361, 222–224. https://doi.org/10.1126/science.aau2405.

Lach, J., Szymonik, A., 2018. Adsorption of diclofenac sodium from aqueous solutions on commercial activated carbons. Desalination Water Treat. 186, 418–429. https://doi.org/10.5004/dwt.2020.25567.

Langmuir, I., 1918. The adsorption of gases on plane surfaces of glass, mica and platinum. J. Am. Chem. Soc. 40, 1361–1403. https://doi.org/10.1021/JA02242A004.

Lazarotto, J.S., da Boit Martinello, K., Georgin, J., Franco, D.S.P., Netto, M.S., Piccilli, D. G.A., Silva, L.F.O., Lima, E.C., Dotto, G.L., 2021. Preparation of activated carbon from the residues of the mushroom (Agaricus bisporus) production chain for the adsorption of the 2,4-dichlorophenoxyacetic herbicide. J. Environ. Chem. Eng. 9, 106843 https://doi.org/10.1016/J.JECE.2021.106843.

Li, X., Wang, C., Zhang, J., Liu, J., Liu, B., Chen, G., 2020. Preparation and application of magnetic biochar in water treatment: a critical review. Sci. Total Environ. 711, 134847 https://doi.org/10.1016/J.SCITOTENV.2019.134847.

Li, K., Zhang, D., Niu, X., Guo, H., Yu, Y., Tang, Z., Lin, Z., Fu, M., 2022. Insights into CO_2 adsorption on KOH-activated biochars derived from the mixed sewage sludge and pine sawdust. Sci. Total Environ. 826, 154133 https://doi.org/10.1016/J.SCITOTENV.2022.154133.

Ligero, A., Calero, M., Pérez, A., Solís, R.R., Muñoz-Batista, M.J., Martín-Lara, M.Á., 2023. Low-cost activated carbon from the pyrolysis of post-consumer plastic waste and the application in CO_2 capture. Process Saf. Environ. Protect. 173, 558–566. https://doi.org/10.1016/J.PSEP.2023.03.041.

Liu, Q., Shi, J., Zheng, S., Tao, M., He, Y., Shi, Y., 2014. Kinetics studies of CO_2 adsorption/desorption on amine-functionalized multiwalled carbon nanotubes. Ind. Eng. Chem. Res. 53, 11677–11683. https://doi.org/10.1021/IE502009N.

Liu, L., Li, W., Song, W., Guo, M., 2018. Remediation techniques for heavy metal-contaminated soils: principles and applicability. Sci. Total Environ. 633, 206–219. https://doi.org/10.1016/J.SCITOTENV.2018.03.161.

Liu, Z., Deng, Z., Davis, S., Ciais, P., 2023. Monitoring global carbon emissions in 2022. Nat. Rev. Earth Environ. 4, 205–206. https://doi.org/10.1038/s43017-023-00406-z.

Lladó, J., Lao-Luque, C., Ruiz, B., Fuente, E., Solé-Sardans, M., Dorado, A.D., 2015. Role of activated carbon properties in atrazine and paracetamol adsorption equilibrium and kinetics. Process Saf. Environ. Protect. 95, 51–59. https://doi.org/10.1016/J.PSEP.2015.02.013.

Lonappan, L., Brar, S.K., Das, R.K., Verma, M., Surampalli, R.Y., 2016. Diclofenac and its transformation products: environmental occurrence and toxicity - a review. Environ. Int. 96, 127–138. https://doi.org/10.1016/J.ENVINT.2016.09.014.

Loos, R., Wollgast, J., Huber, T., Hanke, G., 2007. Polar herbicides, pharmaceutical products, perfluorooctanesulfonate (PFOS), perfluorooctanoate (PFOA), and nonylphenol and its carboxylates and ethoxylates in surface and tap waters around Lake Maggiore in Northern Italy. Anal. Bioanal. Chem. 387, 1469–1478. https://doi.org/10.1007/S00216-006-1036-7.

López, J., Gibert, O., Cortina, J.L., 2023. The role of nanofiltration modelling tools in the design of sustainable valorisation of metal-influenced acidic mine waters: the Aznalcóllar open-pit case. Chem. Eng. J. 451, 138947 https://doi.org/10.1016/J.CEJ.2022.138947.

Lu, K., Yang, X., Gielen, G., Bolan, N., Ok, Y.S., Niazi, N.K., Xu, S., Yuan, G., Chen, X., Zhang, X., Liu, D., Song, Z., Liu, X., Wang, H., 2017. Effect of bamboo and rice straw biochars on the mobility and redistribution of heavy metals (Cd, Cu, Pb and Zn) in contaminated soil. J. Environ. Manag. 186, 285–292. https://doi.org/10.1016/J.JENVMAN.2016.05.068.

Malhotra, M., Suresh, S., Garg, A., 2018. Tea waste derived activated carbon for the adsorption of sodium diclofenac from wastewater: adsorbent characteristics, adsorption isotherms, kinetics, and thermodynamics. Environ. Sci. Pollut. Control Ser. 25, 32210–32220. https://doi.org/10.1007/S11356-018-3148-Y.

Manning, W.J., 2010. Plants in urban ecosystems: essential role of urban forests in urban metabolism and succession toward sustainability. Int. J. Sustain. Dev. World Ecol. 15, 362–370. https://doi.org/10.3843/SUSDEV.15.4:12.

Mariana, M., Abdul, A.K., Mistar, E.M., Yahya, E.B., Alfatah, T., Danish, M., Amayreh, M., 2021. Recent advances in activated carbon modification techniques for enhanced heavy metal adsorption. J. Water Proc. Eng. 43, 102221 https://doi.org/10.1016/J.JWPE.2021.102221.

Mengesha, D.N., Abebe, M.W., Appiah-Ntiamoah, R., Kim, H., 2022. Ground coffee waste-derived carbon for adsorptive removal of caffeine: effect of surface chemistry and porous structure. Sci. Total Environ. 818, 151669 https://doi.org/10.1016/J.SCITOTENV.2021.151669.

Moussa, M., Bader, N., Querejeta, N., Durán, I., Pevida, C., Ouederni, A., 2017. Toward sustainable hydrogen storage and carbon dioxide capture in post-combustion conditions. J. Environ. Chem. Eng. 5, 1628–1637. https://doi.org/10.1016/J.JECE.2017.03.003.

Mozaffari Majd, M., Kordzadeh-Kermani, V., Ghalandari, V., Askari, A., Sillanpää, M., 2022. Adsorption isotherm models: a comprehensive and systematic review (2010−2020). Sci. Total Environ. 812, 151334 https://doi.org/10.1016/J.SCITOTENV.2021.151334.

Mukherjee, I., Singh, U.K., Singh, R.P., 2021. An overview on heavy metal contamination of water system and sustainable approach for remediation. In: Water Pollution and Management Practices. Springer Singapore, pp. 255–277. https://doi.org/10.1007/978-981-15-8358-2_11.

Muya, F.N., Sunday, C.E., Baker, P., Iwuoha, E., 2016. Environmental remediation of heavy metal ions from aqueous solution through hydrogel adsorption: a critical review. Water Sci. Technol. 73, 983–992. https://doi.org/10.2166/WST.2015.567.

Nakkasunchi, S., Hewitt, N.J., Zoppi, C., Brandoni, C., 2021. A review of energy optimization modelling tools for the decarbonisation of wastewater treatment plants. J. Clean. Prod. 279, 123811 https://doi.org/10.1016/J.JCLEPRO.2020.123811.

Nguyen, D.T., Tran, H.N., Juang, R.S., Dat, N.D., Tomul, F., Ivanets, A., Woo, S.H., Hosseini-Bandegharaei, A., Nguyen, V.P., Chao, H.P., 2020. Adsorption process and mechanism of acetaminophen onto commercial activated carbon. J. Environ. Chem. Eng. 8, 104408 https://doi.org/10.1016/J.JECE.2020.104408.

Nuhnen, A., Janiak, C., 2020. A practical guide to calculate the isosteric heat/enthalpy of adsorption via adsorption isotherms in metal–organic frameworks, MOFs. Dalton Trans. 49, 10295–10307. https://doi.org/10.1039/D0DT01784A.

Odunlami, O.A., Vershima, D.A., Oladimeji, T.E., Nkongho, S., Ogunlade, S.K., Fakinle, B.S., 2022. Advanced techniques for the capturing and separation of CO_2 – a review. Results in EngResults in Eng 15, 100512. https://doi.org/10.1016/J.RINENG.2022.100512.

Pérez-Huertas, S., Calero, M., Ligero, A., Pérez, A., Terpiłowski, K., Martín-Lara, M.A., 2023. On the use of plastic precursors for preparation of activated carbons and their evaluation in CO_2 capture for biogas upgrading: a review. Waste Manag. 161, 116–141. https://doi.org/10.1016/J.WASMAN.2023.02.022.

Phong Vo, H.N., Le, G.K., Hong Nguyen, T.M., Bui, X.T., Nguyen, K.H., Rene, E.R., Vo, T. D.H., Thanh Cao, N.D., Mohan, R., 2019. Acetaminophen micropollutant: historical and current occurrences, toxicity, removal strategies and transformation pathways in different environments. Chemosphere 236, 124391. https://doi.org/10.1016/J.CHEMOSPHERE.2019.124391.

Pigatto, R.S., Franco, D.S.P., Netto, M.S., Carissimi, É., Oliveira, L.F.S., Jahn, S.L., Dotto, G.L., 2020. An eco-friendly and low-cost strategy for groundwater defluorination: adsorption of fluoride onto calcinated sludge. J. Environ. Chem. Eng. 8, 104546 https://doi.org/10.1016/J.JECE.2020.104546.

Plaza, M.G., González, A.S., Pis, J.J., Rubiera, F., Pevida, C., 2014. Production of microporous biochars by single-step oxidation: effect of activation conditions on CO_2 capture. Appl. Energy 114, 551–562. https://doi.org/10.1016/J.APENERGY.2013.09.058.

Portinho, R., Zanella, O., Féris, L.A., 2017. Grape stalk application for caffeine removal through adsorption. J. Environ. Manag. 202, 178–187. https://doi.org/10.1016/J.JENVMAN.2017.07.033.

Pylypchuk, I.V., Kessler, V.G., Seisenbaeva, G.A., 2018. Simultaneous removal of acetaminophen, diclofenac, and Cd(II) by Trametes versicolor laccase immobilized on Fe_3O_4/SiO_2-DTPA hybrid nanocomposites. ACS Sustain. Chem. Eng. 6, 9979–9989. https://doi.org/10.1021/ACSSUSCHEMENG.8B01207.

Quan, C., Zhou, Y., Wang, J., Wu, C., Gao, N., 2023. Biomass-based carbon materials for CO_2 capture: a review. J. CO2 Util. 68, 102373 https://doi.org/10.1016/J.JCOU.2022.102373.

Ramírez-Valencia, L.D., Bailón-García, E., Moral-Rodríguez, A.I., Carrasco-Marín, F., Pérez-Cadenas, A.F., 2023. Carbon gels–green graphene composites as metal-free bifunctional electro-fenton catalysts. Gels 9, 665. https://doi.org/10.3390/GELS9080665.

Ramos, V.C., Han, W., Zhang, X., Zhang, S., Yeung, K.L., 2020. Supported ionic liquids for air purification. Curr Opin Green Sustain Chem 25, 100391. https://doi.org/10.1016/J.COGSC.2020.100391.

Rathi, B.S., Kumar, P.S., Vo, D.V.N., 2021. Critical review on hazardous pollutants in water environment: occurrence, monitoring, fate, removal technologies and risk assessment. Sci. Total Environ. 797, 149134 https://doi.org/10.1016/J.SCITOTENV.2021.149134.

Resasco, D.E., Crossley, S.P., Wang, B., White, J.L., 2021. Interaction of water with zeolites: a review. Catal. Rev. 63, 302–362. https://doi.org/10.1080/01614940.2021.1948301.

Ruiz, B., Cabrita, I., Mestre, A.S., Parra, J.B., Pires, J., Carvalho, A.P., Ania, C.O., 2010. Surface heterogeneity effects of activated carbons on the kinetics of paracetamol removal from aqueous solution. Appl. Surf. Sci. 256, 5171–5175. https://doi.org/10.1016/J.APSUSC.2009.12.086.

Sakhiya, A.K., Anand, A., Kaushal, P., 2020. Production, activation, and applications of biochar in recent times. Biochar 2 (3 2), 253–285. https://doi.org/10.1007/S42773-020-00047-1, 2020.

Saleem, H., Khan, M.B., Shabbir, M.S., Khan, G.Y., Usman, M., 2022. Nexus between non-renewable energy production, CO_2 emissions, and healthcare spending in OECD

economies. Environ. Sci. Pollut. Control Ser. 29, 47286–47297. https://doi.org/10.1007/S11356-021-18131-9.
Saleh, T.A., 2022. Adsorption technology and surface science. Interface Science and Technology 34, 39–64. https://doi.org/10.1016/B978-0-12-849876-7.00006-3.
Salomón, Y.L.D.O., Georgin, J., Franco, D.S.P., Netto, M.S., Piccilli, D.G.A., Foletto, E.L., Oliveira, L.F.S., Dotto, G.L., 2021. High-performance removal of 2,4-dichlorophenoxyacetic acid herbicide in water using activated carbon derived from Queen palm fruit endocarp (Syagrus romanzoffiana). J. Environ. Chem. Eng. 9, 104911 https://doi.org/10.1016/J.JECE.2020.104911.
Sarici-Özdemir, Ç., Önal, Y., 2016. Study to observe the applicability of the adsorption isotherms used for the adsorption of medicine organics onto activated carbon. Part. Sci. Technol. 36, 254–261. https://doi.org/10.1080/02726351.2016.1246497.
Sellaoui, L., Silva, L.F.O., Badawi, M., Ali, J., Favarin, N., Dotto, G.L., Erto, A., Chen, Z., 2021. Adsorption of ketoprofen and 2- nitrophenol on activated carbon prepared from winery wastes: a combined experimental and theoretical study. J. Mol. Liq. 333, 115906 https://doi.org/10.1016/J.MOLLIQ.2021.115906.
Sellaoui, L., Gómez-Avilés, A., Dhaouadi, F., Bedia, J., Bonilla-Petriciolet, A., Rtimi, S., Belver, C., 2023. Adsorption of emerging pollutants on lignin-based activated carbon: analysis of adsorption mechanism via characterization, kinetics and equilibrium studies. Chem. Eng. J. 452, 139399 https://doi.org/10.1016/J.CEJ.2022.139399.
Serafin, J., Dziejarski, B., 2023. Application of isotherms models and error functions in activated carbon CO_2 sorption processes. Microporous Mesoporous Mater. 354, 112513 https://doi.org/10.1016/J.MICROMESO.2023.112513.
Serna-Guerrero, R., Sayari, A., 2010. Modeling adsorption of CO_2 on amine-functionalized mesoporous silica. 2: kinetics and breakthrough curves. Chem. Eng. J. 161, 182–190. https://doi.org/10.1016/J.CEJ.2010.04.042.
Sevilla, M., Díez, N., Fuertes, A.B., 2021. More sustainable chemical activation strategies for the production of porous carbons. ChemSusChem 14, 94–117. https://doi.org/10.1002/CSSC.202001838.
Shafeeyan, M.S., Daud, W.M.A.W., Houshmand, A., Shamiri, A., 2010. A review on surface modification of activated carbon for carbon dioxide adsorption. J. Anal. Appl. Pyrolysis 89, 143–151. https://doi.org/10.1016/J.JAAP.2010.07.006.
Shafeeyan, M.S., Daud, W.M.A.W., Shamiri, A., Aghamohammadi, N., 2015. Modeling of carbon dioxide adsorption onto ammonia-modified activated carbon: kinetic analysis and breakthrough behavior. Energy Fuel. 29, 6565–6577. https://doi.org/10.1021/ACS.ENERGYFUELS.5B00653.
Sing, K.S.W., Everett, D.H., Haul, R.A.W., Moscou, L., Pierotti, R.A., Rouquerol, J., Siemieniewska, T., 1985. Reporting physisorption data for gas/solid systems with special reference to the determination of surface area and porosity. Pure Appl. Chem. 57, 603–619. https://doi.org/10.1351/PAC198557040603.
Singh, V.K., Anil Kumar, E., 2016. Measurement and analysis of adsorption isotherms of CO_2 on activated carbon. Appl. Therm. Eng. 97, 77–86. https://doi.org/10.1016/J.APPLTHERMALENG.2015.10.052.
Sips, R., 1948. On the structure of a catalyst surface. J. Chem. Phys. 16, 490–495. https://doi.org/10.1063/1.1746922.
Song, X., Wang, L., Gong, J., Zhan, X., Zeng, Y., 2020. Exploring a new method to study the effects of surface functional groups on adsorption of CO_2 and CH_4 on activated carbons. Langmuir 36, 3862–3870. https://doi.org/10.1021/ACS.LANGMUIR.9B03475.
Sophia A, C., Lima, E.C., 2018. Removal of emerging contaminants from the environment by adsorption. Ecotoxicol. Environ. Saf. 150, 1–17. https://doi.org/10.1016/J.ECOENV.2017.12.026.
Sotelo, J.L., Rodríguez, A., Álvarez, S., García, J., 2012. Removal of caffeine and diclofenac on activated carbon in fixed bed column. Chem. Eng. Res. Des. 90, 967–974. https://doi.org/10.1016/J.CHERD.2011.10.012.
Spessato, L., Bedin, K.C., Cazetta, A.L., Souza, I.P.A.F., Duarte, V.A., Crespo, L.H.S., Silva, M.C., Pontes, R.M., Almeida, V.C., 2019. KOH-super activated carbon from biomass waste: insights into the paracetamol adsorption mechanism and thermal regeneration cycles. J. Hazard Mater. 371, 499–505. https://doi.org/10.1016/J.JHAZMAT.2019.02.102.
Srivastava, A., Gupta, B., Majumder, A., Gupta, A.K., Nimbhorkar, S.K., 2021. A comprehensive review on the synthesis, performance, modifications, and regeneration of activated carbon for the adsorptive removal of various water pollutants. J. Environ. Chem. Eng. 9, 106177 https://doi.org/10.1016/J.JECE.2021.106177.
Stevens, L., Williams, K., Han, W.Y., Drage, T., Snape, C., Wood, J., Wang, J., 2013. Preparation and CO_2 adsorption of diamine modified montmorillonite via exfoliation grafting route. Chem. Eng. J. 215–216, 699–708. https://doi.org/10.1016/J.CEJ.2012.11.058.
Streit, A.F.M., Collazzo, G.C., Druzian, S.P., Verdi, R.S., Foletto, E.L., Oliveira, L.F.S., Dotto, G.L., 2021. Adsorption of ibuprofen, ketoprofen, and paracetamol onto activated carbon prepared from effluent treatment plant sludge of the beverage industry. Chemosphere 262, 128322. https://doi.org/10.1016/J.CHEMOSPHERE.2020.128322.
Tan, K.L., Hameed, B.H., 2017. Insight into the adsorption kinetics models for the removal of contaminants from aqueous solutions. J. Taiwan Inst. Chem. Eng. 74, 25–48. https://doi.org/10.1016/J.JTICE.2017.01.024.
Torrellas, S.Á., García Lovera, R., Escalona, N., Sepúlveda, C., Sotelo, J.L., García, J., 2015. Chemical-activated carbons from peach stones for the adsorption of emerging contaminants in aqueous solutions. Chem. Eng. J. 279, 788–798. https://doi.org/10.1016/J.CEJ.2015.05.104.
Ungureanu, N., Vlăduț, V., Voicu, G., 2020. Water scarcity and wastewater reuse in crop irrigation. Sustainability 12, 9055. https://doi.org/10.3390/SU12219055.
Wang, J., Guo, X., 2020. Adsorption kinetic models: physical meanings, applications, and solving methods. J. Hazard Mater. 390, 122156 https://doi.org/10.1016/J.JHAZMAT.2020.122156.
Wang, Z., Luo, P., Zha, X., Xu, C., Kang, S., Zhou, M., Nover, D., Wang, Y., 2022a. Overview assessment of risk evaluation and treatment technologies for heavy metal pollution of water and soil. J. Clean. Prod. 379, 134043 https://doi.org/10.1016/J.JCLEPRO.2022.134043.
Wang, S., Lee, Y.R., Won, Y., Kim, H., Jeong, S.E., Wook Hwang, B., Ra Cho, A., Kim, J.Y., Cheol Park, Y., Nam, H., Lee, D.H., Kim, H., Jo, S.H., 2022b. Development of high-performance adsorbent using KOH-impregnated rice husk-based activated carbon for indoor CO_2 adsorption. Chem. Eng. J. 437, 135378 https://doi.org/10.1016/J.CEJ.2022.135378.
Wei, M., Yu, Q., Xie, H., Zuo, Z., Hou, L., Yang, F., 2017. Kinetics studies of CO_2 adsorption and desorption on waste ion-exchange resin-based activated carbon. Int. J. Hydrogen Energy 42, 27122–27129. https://doi.org/10.1016/J.IJHYDENE.2017.09.102.
Wei, R., Dai, X., Shi, F., 2019. Enhanced CO_2 adsorption on nitrogen-doped carbon materials by salt and base Co-activation method. Materials 12, 1207. https://doi.org/10.3390/MA12081207.
Yadav, D., Rangabhashiyam, S., Verma, P., Singh, P., Devi, P., Kumar, P., Hussain, C.M., Gaurav, G.K., Kumar, K.S., 2021. Environmental and health impacts of contaminants of emerging concerns: recent treatment challenges and approaches. Chemosphere 272, 129492. https://doi.org/10.1016/J.CHEMOSPHERE.2020.129492.
Yaumi, A.L., Bakar, M.Z.A., Hameed, B.H., 2018. Melamine-nitrogenated mesoporous activated carbon derived from rice husk for carbon dioxide adsorption in fixed-bed. Energy 155, 46–55. https://doi.org/10.1016/J.ENERGY.2018.04.183.
Zanella, H.G., Spessato, L., Lopes, G.K.P., Yokoyama, J.T.C., Silva, M.C., Souza, P.S.C., Ronix, A., Cazetta, A.L., Almeida, V.C., 2021. Caffeine adsorption on activated biochar derived from macrophytes (Eichornia crassipes). J. Mol. Liq. 340, 117206 https://doi.org/10.1016/J.MOLLIQ.2021.117206.
Zhang, X.Q., Li, W.C., Lu, A.H., 2015. Designed porous carbon materials for efficient CO_2 adsorption and separation. N. Carbon Mater. 30, 481–501. https://doi.org/10.1016/S1872-5805(15)60203-7.